# Dear Author

Here are the proofs of your article.

- You can submit your corrections **online,** via **e-mail** or by **fax**.
- For **online** submission please insert your corrections in the online correction form. Always indicate the line number to which the correction refers.
- You can also insert your corrections in the proof PDF and **email** the annotated PDF.
- For **fax** submission, please ensure that your corrections are clearly legible. Use a fine black pen and write the correction in the margin, not too close to the edge of the page.
- Remember to note the **journal title**, **article number**, and **your name** when sending your response via e-mail or fax.
- **Check** the metadata sheet to make sure that the header information, especially author names and the corresponding affiliations are correctly shown.
- **Check** the questions that may have arisen during copy editing and insert your answers/corrections.
- **Check** that the text is complete and that all figures, tables and their legends are included. Also check the accuracy of special characters, equations, and electronic supplementary material if applicable. If necessary refer to the *Edited manuscript*.
- The publication of inaccurate data such as dosages and units can have serious consequences. Please take particular care that all such details are correct.
- Please **do not** make changes that involve only matters of style. We have generally introduced forms that follow the journal's style.
- Substantial changes in content, e.g., new results, corrected values, title and authorship are not allowed without the approval of the responsible editor. In such a case, please contact the Editorial Office and return his/her consent together with the proof.
- If we do not receive your corrections **within 48 hours**, we will send you a reminder.
- Your article will be published **Online First** approximately one week after receipt of your corrected proofs. This is the **official first publication** citable with the DOI. **Further changes are, therefore, not possible.**
- The **printed version** will follow in a forthcoming issue.

**Please note**

After online publication, subscribers (personal/institutional) to this journal will have access to the complete article via the DOI using the URL:
http://dx.doi.org/10.1007/s12237-018-0410-y

If you would like to know when your article has been published online, take advantage of our free alert service. For registration and further information, go to: http://www.link.springer.com.

Due to the electronic nature of the procedure, the manuscript and the original figures will only be returned to you on special request. When you return your corrections, please inform us, if you would like to have these documents returned.

AUTHOR'S PROOF

# Metadata of the article that will be visualized in OnlineFirst

Please note: Images will appear in color online but will be printed in black and white.

| | | | |
|---|---|---|---|
| 1 | Article Title | **Effects of Tidal-Forcing Variations on Tidal Properties Along a Narrow Convergent Estuary** | |
| 2 | Article Sub-Title | | |
| 3 | Article Copyright - Year | **Coastal and Estuarine Research Federation 2018 (This will be the copyright line in the final PDF)** | |
| 4 | Journal Name | Estuaries and Coasts | |
| 5 | Corresponding Author | Family Name | **Cai** |
| 6 | | Particle | |
| 7 | | Given Name | **Huayang** |
| 8 | | Suffix | |
| 9 | | Organization | Sun Yat-sen University |
| 10 | | Division | Institute of Estuarine and Coastal Research, School of Marine Sciences |
| 11 | | Address | Guangzhou, 510275, China |
| 12 | | Organization | Guangdong Provincial Key Laboratory of Marine Resources and Coastal Engineering |
| 13 | | Division | |
| 14 | | Address | Guangzhou, 510275, China |
| 15 | | e-mail | caihy7@mail.sysu.edu.cn |
| 16 | Author | Family Name | **Garel** |
| 17 | | Particle | |
| 18 | | Given Name | **Erwan** |
| 19 | | Suffix | |
| 20 | | Organization | University of Algarve |
| 21 | | Division | Centre for Marine and Environmental Research (CIMA) |
| 22 | | Address | Faro, Portugal |
| 23 | | e-mail | None |
| 24 | Schedule | Received | 31 October 2017 |
| 25 | | Revised | 18 April 2018 |
| 26 | | Accepted | 20 April 2018 |
| 27 | Abstract | A 1D analytical framework is implemented in a narrow convergent estuary that is 78 km in length (the Guadiana, Southern Iberia) to evaluate the tidal dynamics along the channel, including the effects of neap-spring amplitude variations at the mouth. The close match between the observations (damping from the mouth to ~ 30 km, shoaling upstream) and outputs from semi-closed channel solutions indicates that the $M_2$ tide is reflected at the estuary head. The model is used to determine the contribution of reflection to the dynamics of the propagating wave. This contribution is mainly confined to the upper one third of the estuary. The relatively | |

constant mean wave height along the channel (< 10% variations) partly results from reflection effects that also modify significantly the wave celerity and the phase difference between tidal velocity and elevation (contradicting the definition of an “ideal” estuary). Furthermore, from the mouth to ~ 50 km, the variable friction experienced by the incident wave at neap and spring tides produces wave shoaling and damping, respectively. As a result, the wave celerity is largest at neap tide along this lower reach, although the mean water level is highest in spring. Overall, the presented analytical framework is useful for describing the main tidal properties along estuaries considering various forcings (amplitude, period) at the estuary mouth and the proposed method could be applicable to other estuaries with small tidal amplitude to depth ratio and negligible river discharge.


| | | |
|---|---|---|
| 28 | Keywords separated by ' - ' | Estuary - Analytical model - Tidal propagation - Wave speed - Resonance - Guadiana |
| 29 | Foot note information | Communicated by Arnoldo Valle-Levinson |

Estuaries and Coasts
https://doi.org/10.1007/s12237-018-0410-y

# Effects of Tidal-Forcing Variations on Tidal Properties Along a Narrow Convergent Estuary

**Erwan Garel[1] · Huayang Cai[2,3]**

Received: 31 October 2017 / Revised: 18 April 2018 / Accepted: 20 April 2018


**Abstract**
A 1D analytical framework is implemented in a narrow convergent estuary that is 78 km in length (the Guadiana, Southern Iberia) to evaluate the tidal dynamics along the channel, including the effects of neap-spring amplitude variations at the mouth. The close match between the observations (damping from the mouth to ∼ 30 km, shoaling upstream) and outputs from semi-closed channel solutions indicates that the $M_2$ tide is reflected at the estuary head. The model is used to determine the contribution of reflection to the dynamics of the propagating wave. This contribution is mainly confined to the upper one third of the estuary. The relatively constant mean wave height along the channel (< 10% variations) partly results from reflection effects that also modify significantly the wave celerity and the phase difference between tidal velocity and elevation (contradicting the definition of an "ideal" estuary). Furthermore, from the mouth to ∼ 50 km, the variable friction experienced by the incident wave at neap and spring tides produces wave shoaling and damping, respectively. As a result, the wave celerity is largest at neap tide along this lower reach, although the mean water level is highest in spring. Overall, the presented analytical framework is useful for describing the main tidal properties along estuaries considering various forcings (amplitude, period) at the estuary mouth and the proposed method could be applicable to other estuaries with small tidal amplitude to depth ratio and negligible river discharge.

**Keywords** Estuary · Analytical model · Tidal propagation · Wave speed · Resonance · Guadiana



## Introduction

Understanding the hydraulic processes that control water elevation and current speed along estuarine channels is essential for many economic and management activities such as navigation, fisheries, and flood protection (Prandle 2009; Savenije 2012). Therefore, many studies have been devoted to understanding the dynamics of tidal waves propagating from the open ocean into estuaries. Accurate simulations can be performed using properly calibrated numerical models. However, numerous runs are usually required to specify the physical drivers of tidal behavior and to gain insights into their sensitivity to variations in the forcing parameters, such as the estuarine geometry, tidal wave characteristics, and friction (see Cai et al. 2016; van Rijn 2011). In line with these goals, various analytical formulations have been developed to address the most important properties of tidal propagation along a channel.

Analytical solutions describing tidal dynamics along estuaries are generally obtained from the derivation of the linearized St. Venant equations, considering idealized channel geometries (Cai et al. 2016, for a brief recapitulation of the most significant contributions, see; Hoitink and Jay 2016; ~~van~~ Rijn 2011). Following this approach, many researchers have provided first-order solutions focusing on the 1D (depth- and cross-section-averaged) aspect of the along channel tidal propagation. Hunt (1964) was one of the first authors to propose such analytical solutions of the linearized equations considering a prismatic channel. Using this approach, the landward decrease in channel cross-sectional area (morphological convergence) is typically considered by dividing the channel into several prismatic sections, each one with its own constant width and

Communicated by Arnoldo Valle-Levinson

✉ Huayang Cai
caihy7@mail.sysu.edu.cn

1 Centre for Marine and Environmental Research (CIMA), University of Algarve, Faro, Portugal

2 Institute of Estuarine and Coastal Research, School of Marine Sciences, Sun Yat-sen University, Guangzhou 510275, China

3 Guangdong Provincial Key Laboratory of Marine Resources and Coastal Engineering, Guangzhou 510275, China

depth (e.g., Dronkers 1964). However, this method, making use of the analytical solution for prismatic channels, is generally not able to accurately represent how convergence affects tidal wave propagation and, in particular, the wave speed since it does not explicitly account for the effect of the estuary convergent shape (Jay 1991). To account more realistically for the estuarine geometry, many authors have analytically solved linearized equations using exponential functions where width and depth variations are represented with single characteristic length-scale parameters (e.g., Friedrichs and Madsen 1992; Prandle and Rahman 1980; Savenije 1998; Winterwerp and Wang 2013). Based on this approach, it is understood that the most important tidal properties in convergent estuaries are controlled by frictional effects, morphological convergence, and reflection, in the case of sharp morphological constrictions, which generally occurs near the head (Friedrichs and Aubrey 1994; Jay 1991; Lanzoni and Seminara 1998; van Rijn 2011). Furthermore, analytical solutions of the 1D St. Venant equations that describe tidal propagation in both infinite and closed-end channels can now be obtained by solving a set of implicit equations that are functions of three parameters accounting for friction, convergence, and channel length (Cai et al. 2016; Savenije et al. 2008; Toffolon and Savenije 2011). This analytical framework requires a few dimensionless input parameters representing the tidal forcing and estuary geometry, independent of the tidal hydrodynamics along the estuary. Despite simplifications inherent to analytical approaches, the results compare remarkably well with numerical model outputs and observations in distinct estuarine settings with or without reflection at the head (e.g., Cai et al. 2012, 2016; Park et al. 2017; Savenije et al. 2008; Savenije and Veling 2005; Zhang et al. 2012).

In general, analytical studies of tidal propagation in estuaries consider multiple tidal constituents to evaluate the effects of tidal forcing variation at the mouth (e.g., Jay et al. 2015; Wang et al. 1999). For example, the $S_2/M_2$ amplitude ratio is useful to represent the transformation of spring-neap wave height asymmetry along a channel, from which the variations of other properties (such as damping rate) can be inferred (e.g., Guo et al. 2015). However, such approach does not explicitly quantify the absolute amplitude and velocity of the propagating wave over the fortnightly cycle. Alternatively, the present paper demonstrates that the analytical framework proposed by Toffolon and Savenije (2011) and Cai et al. (2016) can be used to explore the tidal forcing variations on tidal dynamics considering a single effective tidal wave rather than multiple constituents. The case study is a narrow convergent estuary (the Guadiana), where the effects of tidal forcing (amplitude, period) variations at the mouth on the propagating wave are directly explored based on a semi-closed-end model calibrated against along-channel observations.



## Overview of the Analytical Model

### Formulation of the Problem

We consider a semi-closed estuary (see Fig. 1) that is forced by a single predominant tidal constituent (e.g., $M_2$) with tidal frequency $\omega = 2\pi/T$, where $T$ is the tidal period. As the tidal wave propagates into the estuary, the main tidal dynamics along the channel can be characterized by a wave celerity of water level $c_A$, a wave celerity of velocity $c_V$, an amplitude of tidal elevation $\eta$, a tidal velocity amplitude $\upsilon$, a phase of water level $\phi_A$, and a phase of velocity $\phi_V$. The length of the estuary is indicated by $L_e$.

Neglecting the nonlinear continuity term $U\partial h/\partial x$ and advective term $U\partial U/\partial x$, the linearized depth-averaged equations for conservation of mass and momentum in a channel with gradually varying cross section can be described by (e.g., Toffolon and Savenije 2011):

$$r_S \frac{\partial h}{\partial t} + h\frac{\partial U}{\partial x} + \frac{hU}{\overline{B}}\frac{\mathrm{d}\overline{B}}{\mathrm{d}x} = 0\,, \tag{1}$$

$$\frac{\partial U}{\partial t} + g\frac{\partial Z}{\partial x} + \frac{rU}{h} = 0\,, \tag{2}$$

where $h$ is the depth, $U$ is the cross-sectionally averaged velocity, $Z$ is the free surface elevation, $r_S$ is the storage width ratio (defined as the ratio of the storage width $B_S$ to the tidally averaged width $\overline{B}$, i.e., $r_S = B_S/\overline{B}$, where hereafter overbars denote tidal averages), $g$ is the gravitational acceleration, $t$ is the time, $x$ is the longitudinal coordinate measured positive in landward direction ($x$=0 at the mouth), and the linearized friction factor $r$ is defined by Lorentz (1926):

$$r = \frac{8}{3\pi}\frac{g\upsilon}{K^2\overline{h}^{1/3}}\,. \tag{3}$$

In Eq. 3, the coefficient $8/(3\pi)$ stems from adopting Lorentz's linearization (Lorentz 1926) of the quadratic friction term considering only one single predominant tidal constituent (e.g., $M_2$), and $K$ is the Manning-Strickler friction coefficient.

To derive the analytical solution for the tidal hydrodynamics, it is assumed that the tidally averaged cross-sectional area $\overline{A}$ and width $\overline{B}$ can be described by the following exponential functions:

$$\overline{A} = \overline{A_0}\exp(-x/a)\,, \tag{4}$$

$$\overline{B} = \overline{B_0}\exp(-x/b)\,, \tag{5}$$

where $\overline{A_0}$ and $\overline{B_0}$ are the respective values at the estuary mouth, and $a$, $b$ are the convergence length of the cross-sectional area and width, respectively. The other fundamental assumption is that the flow is mainly concentrated in a rectangular cross section, with a possible influence from

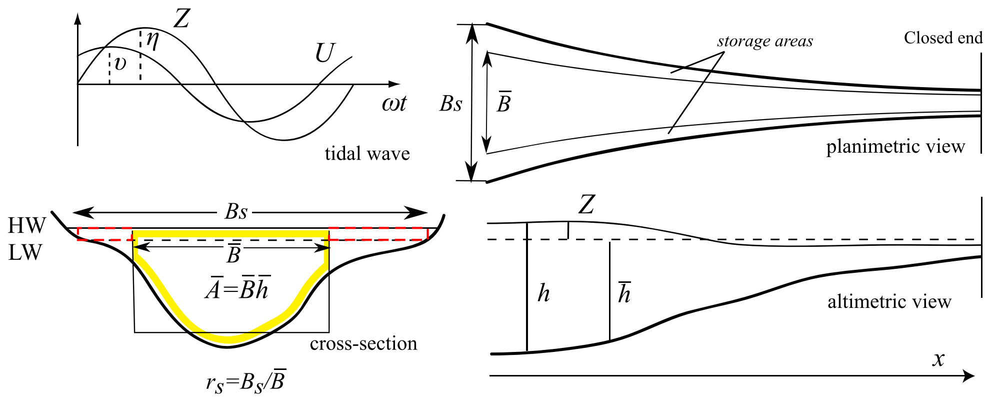


**Fig. 1** Geometry of a semi-closed estuary and basic notation (after Savenije et al. 2008). *HW*, high water; *LW*, low water

storage areas described by the storage width ratio $r_S$ (see Fig. 1). It directly follows from the assumption of a rectangular cross section that the tidally averaged depth is given by $\overline{h} = \overline{A}/\overline{B}$.

In order to recast the problem in dimensionless form, we define the parameters with reference to the scales at the estuary mouth (denoted by the subscript 0), including the tidally averaged depth $\overline{h_0}$, width $\overline{B_0}$, and tidal amplitude $\eta_0$. The natural length scale is the frictionless tidal wave length in a prismatic channel $L_0$, which is defined as $c_0/\omega$, where $c_0 = \sqrt{g\overline{h_0}/r_S}$ is the classical wave celerity in a frictionless prismatic channel. It was shown by Toffolon and Savenije (2011) and Cai et al. (2016) that in principle, the tidal hydrodynamics along the estuary axis are mainly determined by four dimensionless parameters (defined in Table 1) that are related to the geometry and external forcing, i.e., $\zeta_0$ the dimensionless tidal amplitude (indicating the seaward boundary condition), $\gamma$ the estuary shape number (representing the effect of the cross-sectional area convergence), $\chi_0$ the friction number (describing the role of frictional dissipation), and $L_e^*$ the dimensionless estuary length (a superscript star hereafter denotes dimensionless variables). The friction number $\chi_0$ is dependent on the Manning-Strickler friction coefficient $K$, which describes the effective friction resulting from various environmental factors that influence the hydraulic drag resistance such as the grain roughness, bedforms, channel geometry, vegetation, and suspended sediments (e.g., Savenije and Veling 2005; Wang et al. 2014; Winterwerp and Wang 2013), and from nonlinear effects induced by secondary astronomical tidal constituents (Prandle 1997). Hence, $K$ is generally problematic to quantify and obtained by calibrating the model results with observations.

The main dependent dimensionless parameters which are used to describe the spatial transformation of the tide are listed in Table 1. Note that these parameters depend on the



**Table 1** The definition of dimensionless parameters

| Dimensionless parameters | |
|---|---|
| Independent | Dependent |
| Tidal amplitude at the mouth | Tidal amplitude |
| $\zeta_0 = \eta_0/\overline{h_0}$ | $\zeta = \eta/\overline{h}$ |
| Friction number at the mouth | Friction number |
| $\chi_0 = r_S c_0 \zeta_0 g/\left(K^2\omega\overline{h_0}^{4/3}\right)$ | $\chi = r_S c_0 \zeta g/\left(K^2\omega\overline{h}^{4/3}\right)$ |
| Estuary shape | Velocity number |
| $\gamma = c_0/(\omega a)$ | $\mu = \upsilon/(r_S\zeta c_0) = \upsilon\overline{h}/(r_S\eta c_0)$ |
| Estuary length | Damping/amplification number for water level |
| $L_e^* = L_e/L_0$ | $\delta_A = c_0 \mathrm{d}\eta/(\eta\omega \mathrm{d}x)$ |
| | Damping/amplification number for velocity |
| | $\delta_V = c_0 \mathrm{d}\upsilon/(\upsilon\omega \mathrm{d}x)$ |
| | Celerity number for water level |
| | $\lambda_A = c_0/c_A$ |
| | Celerity number for velocity |
| | $\lambda_V = c_0/c_V$ |
| | Phase lead |
| | $\phi = \phi_V - \phi_A$ |

resulting tidal motion in the channel (mainly because they are concerned with the velocity). In particular, the reference scale for the velocity is given by $r_S \zeta_0 c_0$. The tidal amplitude $\zeta$ and friction number $\chi$ consist of actual (i.e., local) values derived from the forcing at the mouth. An increasing friction number represents an increasing contribution of frictional dissipation ($\chi = 0$ in a frictionless case). The velocity number $\mu$ is the ratio of the actual velocity amplitude to the frictionless value in a prismatic channel. The celerity number for elevation $\lambda_A$ and velocity $\lambda_V$ is defined as the ratio between the frictionless wave celerity in a prismatic channel ($c_0$) and the actual wave celerity $c$ (i.e., it is $<1$ for waves faster than $c_0$). The damping/amplification number for elevation $\delta_A$ and velocity $\delta_V$ describes the rate of increase, $\delta_A$ (or $\delta_V$) $> 0$, or decrease $\delta_A$ (or $\delta_V$) $< 0$ of the wave amplitudes along the estuary axis. The phase difference between velocity and elevation is $\phi = \phi_V - \phi_A$, equals to 0 for a purely progressive wave, and referred to as the "phase lead" hereafter (Van Rijn 2010).

## Analytical Solutions for Tidal Hydrodynamics

In this study, the analytical solutions for tidal hydrodynamics in a semi-closed tidal channel previously developed by Toffolon and Savenije (2011) (see also Cai et al. 2016) were adopted to reproduce the longitudinal tidal dynamics along the channel axis. Concentrating on the propagation of one predominant tidal constituent (e.g., $M_2$), the solutions for $U$ and $Z$ can be expressed as follows:

$$Z = \eta \cos(\omega t + \phi_A) = \zeta_0 \overline{h_0} [A^* \exp(i\omega t) + cc]/2 , \quad (6)$$

$$U = \upsilon \cos(\omega t + \phi_V) = r_S \zeta_0 c_0 [V^* \exp(i\omega t) + cc]/2 , \quad (7)$$

where $A^*$ and $V^*$ are complex functions of amplitudes that vary along the dimensionless coordinate $x^* = x/L_0$ (cc represents the complex conjugate of the preceding term):

$$A^* = a_1^* \exp\left(w_1^* x^*\right) + a_2^* \exp\left(w_2^* x^*\right) , \quad (8)$$

$$V^* = \upsilon_1^* \exp\left(w_1^* x^*\right) + \upsilon_2^* \exp\left(w_2^* x^*\right) . \quad (9)$$

For a channel forced by the tide at the seaward boundary and closed landward, the analytical solutions for the unknown variables in Eqs. 8 and (9) are given by

$$a_1^* = \left[1 + \exp\left(\Lambda L^*\right) \frac{\Lambda + \gamma/2}{\Lambda - \gamma/2}\right]^{-1} ,$$
$$\upsilon_1^* = \frac{-i a_1^*}{\Lambda - \gamma/2} , \qquad w_1^* = \gamma/2 + \Lambda , \quad (10)$$

$$a_2^* = 1 - a_1^* , \qquad \upsilon_2^* = \frac{i(1 - a_1^*)}{\Lambda + \gamma/2} , \qquad w_2^* = \gamma/2 - \Lambda , \quad (11)$$

where $\Lambda$ is a complex variable, defined as follows:

$$\Lambda = \sqrt{\gamma^2/4 - 1 + i\widehat{\chi}} , \qquad \widehat{\chi} = \frac{8}{3\pi}\mu\chi , \quad (12)$$

and $L^*$ is the distance to the head of the estuary:

$$L^* = L_e^* - x^* . \quad (13)$$

In particular, $w_l^* = m_l^* + i k_l^* (l{=}1,2)$ is a complex number, with $m_l^*$ representing the amplification factor and $k_l^*$ the wave number.

An infinitely long estuarine channel is characterized by a length $L^*$ approaching infinity, which is an asymptotic solution for a semi-closed channel. In this case, the analytical solution can be determined by imposing the landward boundary condition at infinity in the semi-closed estuary model, where the unknown complex variables are given by the following:

$$a_1^* = 0 , \qquad a_2^* = 1 , \qquad \upsilon_1^* = 0 , \qquad \upsilon_2^* = \frac{i}{\Lambda + \gamma/2} . \quad (14)$$

The first terms on the right-hand side of Eqs. 8 and (9) represent a wave traveling seaward (i.e., reflected wave), while the second terms represent a wave traveling landward (i.e., incident wave). As a result, the reflection coefficients $\Psi_A$ for tidal amplitude (the ratio of the amplitude of the reflected to incident wave) and $\Psi_V$ for velocity amplitude can be described by the following:

$$\Psi_A = \left|\frac{a_1^*}{a_2^*}\right| , \qquad \Psi_V = \left|\frac{\upsilon_1^*}{\upsilon_2^*}\right| , \quad (15)$$

where vertical bars indicate the absolute values.

It was shown by Toffolon and Savenije (2011) that the amplitudes $a_1^*$, $a_2^*$ and $\upsilon_1^*$, $\upsilon_2^*$ (and hence $A^*$ and $V^*$) are determined by means of suitable boundary conditions imposed at the channel ends, i.e., the tidal forcing imposed at the seaward boundary (corresponding to $a_1^*$ and $a_2^*$) and a closed channel in the landward boundary (corresponding to $\upsilon_1^*$ and $\upsilon_2^*$). For given computed $A^*$ and $V^*$, the analytical solutions for the tidal wave amplitudes and their corresponding phases, which are defined by Eqs. 6 and 7, are as follows:

$$\eta = \zeta_0 \, \overline{h_0} \, |A^*| , \qquad \upsilon = r_S \, \zeta_0 \, c_0 \, |V^*| , \quad (16)$$

$$\tan(\phi_A) = \frac{\Im(A^*)}{\Re(A^*)} , \qquad \tan(\phi_V) = \frac{\Im(V^*)}{\Re(V^*)} , \quad (17)$$

where $\Re$ and $\Im$ are the real and imaginary parts of the corresponding term.

On the other hand, the dependent parameters defined in Table 1 can be calculated using the computed $\eta$ and $\upsilon$ from Eq. 16. Alternatively, the dimensionless parameters of velocity scale $\mu$, the damping/amplification $\delta_A$, $\delta_V$ and celerity numbers $\lambda_A$, $\lambda_V$ of the waves can be expressed as follows (Toffolon and Savenije 2011):

$$\mu = |V^*|, \tag{18}$$

$$\delta_A = \Re\left(\frac{1}{A^*}\frac{dA^*}{dx^*}\right), \qquad \delta_V = \Re\left(\frac{1}{V^*}\frac{dV^*}{dx^*}\right), \tag{19}$$

$$\lambda_A = \Im\left(\frac{1}{A^*}\frac{dA^*}{dx^*}\right), \qquad \lambda_V = \Im\left(\frac{1}{V^*}\frac{dV^*}{dx^*}\right). \tag{20}$$

Note that the dimensionless friction parameter $\widehat{\chi}$ defined in Eq. 12 depends on the unknown value of the velocity scale $\mu$ (or $\upsilon$). Thus, an iterative procedure is needed to determine the correct wave behavior. Furthermore, to account for the longitudinal variation of the cross-sections (longitudinal channel width and depth), the entire channel was subdivided into multiple reaches. The solutions were then obtained by solving a set of linear equations, with internal boundary conditions at the junction of the sub-reaches satisfying the continuity condition (i.e., the continuous water level and discharge, for details, see Cai et al. 2016; Toffolon and Savenije 2011).

## Study Site and Data

The Guadiana is a 78-km-long estuary in southern Iberia consisting of a single channel running from a weir (Moinho do Canais) at the head to the Gulf of Cadiz (Fig. 2). The semi-diurnal tide at the mouth is regular and meso-tidal, with a mean range of 2 m (1.3 and 2.6 m on

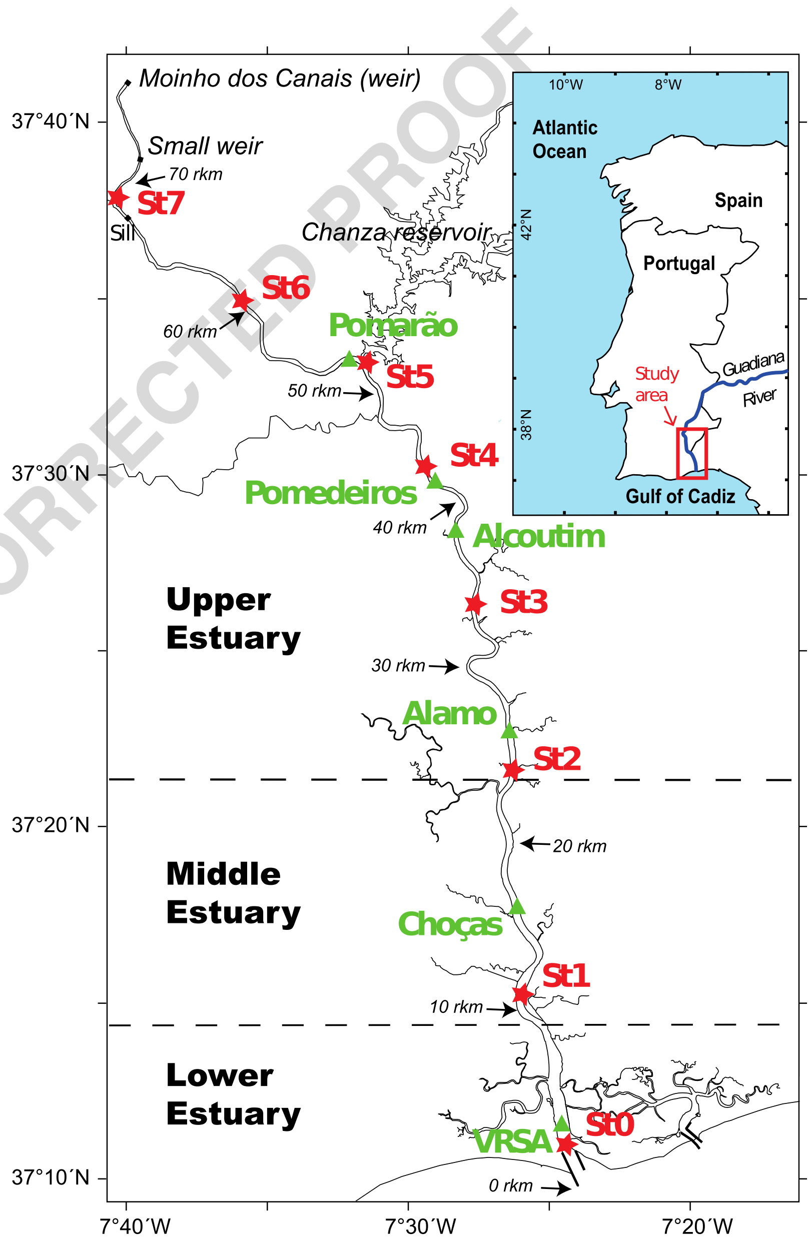


**Fig. 2** Map of the Guadiana Estuary (for general location, see inset) with the locations of the pressure transducer Stations (red stars, St0-7) and velocity measurements (green triangles, named for nearby localities). VRSA, Vila Real de Santo Antonio

average at neap and spring tides, respectively). In this study, locations along the estuary are reported in river kilometers (rkm) measured landward from the seaward extremity of the western jetty at the mouth (which is at 0 rkm; see Fig. 2). Three sectors are distinguished based on distinct eco-hydrological characteristics: the upper estuary, from the head to 23 rkm, which is generally filled up with freshwater; the middle estuary, from 23 to 7 rkm, which is characterized by brackish water; and the lower estuary which includes the terminal seaward section that is strongly influenced by seawater (Fig. 2).

Along its upper and middle sectors, the estuary is confined into a deep and narrow valley incised in the bedrock. Only the lower estuary is embedded in soft sediment, allowing for the development of limited salt marsh areas (about 20 km$^2$, only). The cross-sectional averaged flow depth varies little, being between 4 and 8 m in general, but is poorly constrained upstream of 50 rkm (Fig. 3). A small weir and a boulder sill lay across the channel within the last 15 km of the estuary (Fig. 2). The mean depth of the entire estuary is approximately 5.5 m. Similar to alluvial (or coastal plain) estuaries, the channel width and cross-sectional area decrease in a landward direction. This evolution can be described by exponential functions (4)–(5) with convergence lengths of $b$ = 38 km for the width and $a$ = 31 km for the cross-sectional area (Fig. 3).

Due to strong dam regulation, the freshwater discharge into the estuary is generally low ($< 50$ m$^3$ s$^{-1}$) throughout the year. Intense local rain falls or episodic water release from dams may produce discharges up to 2500 m$^3$ s$^{-1}$ lasting from a few days up to a few weeks. These events occur unfrequently, mainly between November and April. In a detailed analysis of riverine contributions into the estuary,

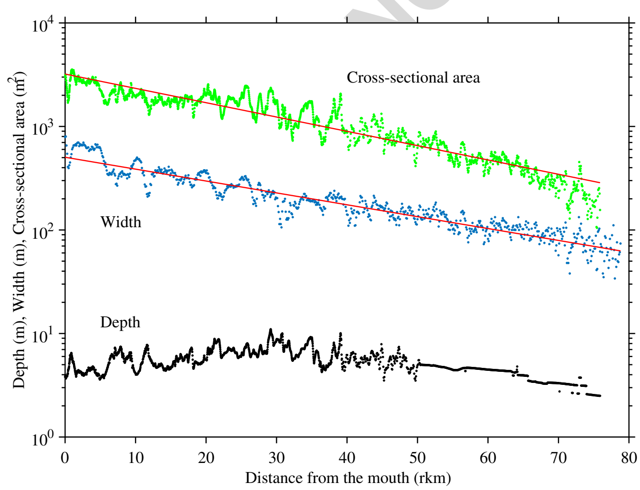


**Fig. 3** Cross-sectional channel area (m$^2$, green dots), width (m, blue dots), and averaged depth (m, black dots) along the Guadiana Estuary. The red lines represent the exponential fit curves for the width and cross-sectional area

Garel and D'Alimonte (2017) reported eight discharge events during a ∼ 40-month period between 2008 and 2014. Under low inflow conditions, the estuary is well mixed at spring tide and weakly stratified at neap tide (see Garel et al. 2009). All of the data presented in this study correspond to periods of low river discharge.

From 31 July to 24 September 2015, a set of eight pressure transducers was deployed every ∼ 10 km along the estuarine channel, from Station 0 (St0) near the mouth to Station 7 (St7) at ∼ 70 rkm (Fig. 2). The raw data, recorded continuously at 1-min intervals, were smoothed with a 10-min moving average window, corrected from atmospheric pressure variations (obtained from a nearby station) and resampled every 10 min. Furthermore, pressure records from a current profiler (Sentinel V, TDRI) deployed in 23 m of water depth over the inner shelf from 4 September to 7 December 2015 provided hourly tidal elevations at 5 km from the mouth.

Fortnightly variability of tidal properties along estuaries is typically assessed implicitly through the $S_2/M_2$ amplitude ratio (e.g., Jay et al. 2015). In the present study, variations in absolute tidal elevation amplitudes at spring and neap tides were obtained directly through demodulation of the tidal signal at each station. The actual tidal amplitude of each tidal cycle was obtained as the difference between consecutive maximum and minimum values of the water level time series interpolated at 1-min interval. The spring tide with largest amplitude (1.7 m on 31 August 2015) and neap tide with weakest amplitude (0.6 m on 23 August 2015) of the records at St0 were selected to exemplify variations in the tidal dynamics in function of the tidal forcing at the mouth. It is worth noting that these amplitudes are close to the regional maxima produced by astronomical tides.

The elevation amplitude ($\eta$) and phase ($\phi_A$) of the tidal constituents were obtained at each station using standard Fourier harmonic analyses of the observed pressure records with the "U-Tide" Matlab package (Codiga 2011). Similarly, the phases of the tidal elevation ($\phi_A$) and velocity ($\phi_V$)—hence the associated phase lead—were derived from older time series collected by the Centre for Marine and Environmental Research (University of Algarve) in the frame of the SIRIA project (see Garel et al. 2009) and SIMPATICO monitoring program (see Garel and Ferreira 2015). These records were obtained with single-point current meters (RCM9) and ADCP current profilers that were bottom-mounted along the estuary for at least 15 days near the deepest part of the channel (for details, see Table 2).

Harmonic analyses are designed for the study of stationary processes and provide here an average of individual tidal constituents over time. In addition, the temporal variability of the tidal signal was analyzed using continuous wavelet transform (CWT). CWT is more accurate and

**Table 2** Current measurements at the Guadiana Estuary that were used in the present study (see also Fig. 2)

| Location | Distance from mouth (rkm) | Instrument | Model | Deployment dates |
|---|---|---|---|---|
| VRSA | 1 | Current profiler | Sontek, XR Argonaut 750 kHz | 20/06/2008–29/03/2009 |
| Chocas | 14 | Current meter | Aanderaa RCM9 | 21/11–06/12/2001 |
| Alamo | 24 | Current meter | Aanderaa RCM9 | 20/11–04/12/2001 |
| Alcoutim | 37 | Current meter | Aanderaa RCM9 | 20/11–04/12/2001 |
| Pomedeiros | 42 | Current profiler | Nortek Aquadopp 1 MHz | 30/12/2005–19/01/2006 |
| Pomarão | 50 | Current meter | Aanderaa RCM9 | 19/11–04/12/2001 |

*VRSA* Vila Real de Santo Antonio

efficient than harmonic analyses for the study of nonstationary phenomena, able to specify the time evolution of the frequency content of a tidal signal (for a description of basic principles, see Jay and Flinchem 1997, 1999). Typically, CWT results are represented here as scaleograms, which are contour plots of amplitude (in m) in function of time (*x*-axis) and frequency (*y*-axis). A limitation of CWT is that it is only able to differentiate tidal species (e.g., the diurnal, semi-diurnal, and quarter-diurnal bands, referred to as $D_1$, $D_2$, and $D_4$, respectively) rather than individual tidal constituents (e.g., $M_2$ and $S_2$). Therefore, harmonic analyses and CWT are often used jointly to resolve nonstationary tides (e.g., Buschman et al. 2009; Flinchem and Jay 2000; Guo et al. 2015; Jay and Flinchem 1997; Jay et al. 2015; Kukulka and Jay 2003; Sassi and Hoitink 2013; Shetye and Vijith 2013). For the study period, the main source of tidal variability at the mouth is the fortnightly cycle resulting from the interaction between the $M_2$ and $S_2$ constituents.

## Results

### Water Level Observations

#### Tidal Wave Amplitude

The mean tidal amplitude at the mouth (St0) was 1.05 m over the study period and varied little (< 10%) along the estuary until St6 (Fig. 4a, black line). Upstream, significant tidal damping occurred due to the bathymetric truncation of the low water level by the sill located between 60 and 70 rkm. The sill height controls the low water level upstream



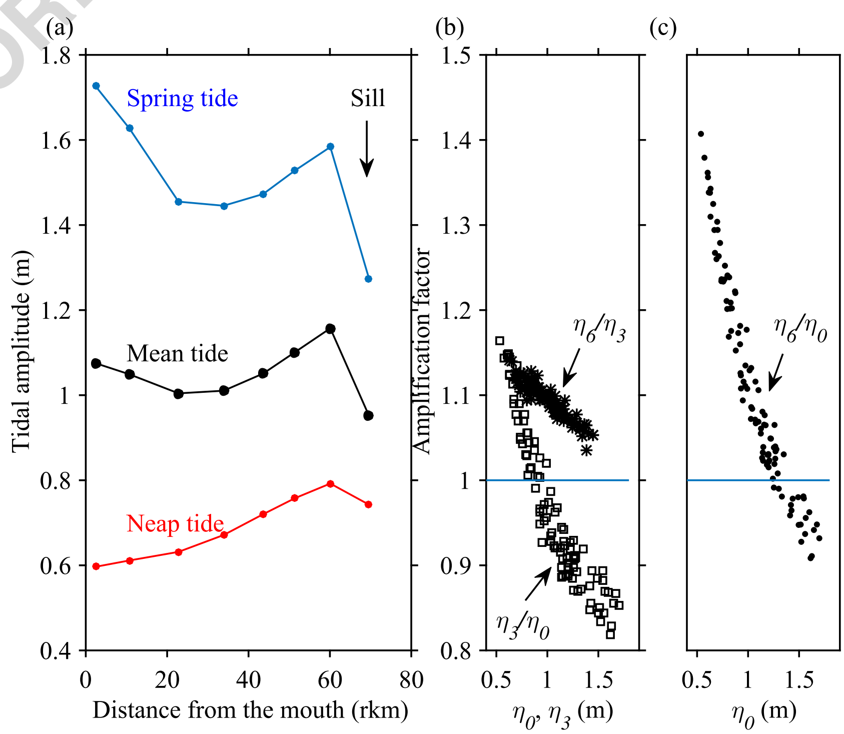


**Fig. 4** **a** Tidal amplitude (m) along the Guadiana Estuary for a mean (black), spring (blue), and neap (red) tide; **b**, **c** amplification factor (>1: amplification; <1: damping) between St0 and St3 (b, squares, $\eta_3/\eta_0$), St3 and St6 (b, circles, $\eta_6/\eta_3$) and St0 and St6 (c, dots, $\eta_6/\eta_0$) in function of the tidal amplitude (m) at the mouth ($\eta_0$) and St3 ($\eta_3$). The vertical arrow indicates the location of a sill between St6 and St7

of the sill, producing an extended falling tide and shortened rising tide at St7 (see Lincoln and FitzGerald 1998). Excluding St7, the tidal wave was moderately damped along the lower and middle estuary and moderately amplified along the upper estuary, reaching a maximum value at St6, which was approximately 10 cm larger than at the mouth.

Significant differences were observed in the tidal height evolution along the estuary in function of the tidal amplitude at the mouth ($\eta_0$). The strong tidal damping between St6 and St7, due to the truncation of the low water levels by the sill, was largest at spring tide (Fig. 4a). This is because the water level is lower at spring than at neap on the seaward side of the sill (e.g., St6; Fig. 5). More importantly, the patterns of tidal propagation were opposite at spring and neap tides along the lower and middle estuary (from 0 to $\sim$ 30 rkm), with a damped and amplified wave at spring tide and neap tide, respectively (Fig. 4a). The amplification factor $\eta_{3/0}$ between St0 and St3 (i.e., the ratio between the tidal amplitudes at St3 and St0) confirms that the wave was amplified at neap tide ($\eta_{3/0} > 1$) but became progressively damped ($\eta_{3/0} < 1$) as the tidal height forcing at the mouth increased towards spring tide values (Fig. 4b, squares). The maximum wave height variation at St3 for a given tide was less than 20% of $\eta_0$ ($1.2 < \eta_{3/0} < 0.8$). By contrast, the tidal wave was always amplified when propagating from St3 to St6 ($\eta_{6/3} > 1$), regardless of the tidal amplitude at the mouth (Fig. 4b, circles). It is noteworthy that the wave height was more amplified at neap tide than at spring tide along this upper portion of the estuary ($\eta_{6/3}$ is approximately 1.15 at neap and 1.05 at spring). Overall, at spring tide the wave was moderately damped between St0 and St6 ($\eta_{6/0}$ slightly less than unity) and a maximum difference in height was observed between the mouth and the middle estuary (e.g., 25 cm between St0 and St3 in Fig. 4a, blue line). At neap tide, the maximum wave amplification (up to 40 %) was observed between St0 and St6 (Fig. 4c); however, the absolute amplification in wave height was modest because of the small tidal amplitude at neap, (e.g., 20-cm amplification between St0 and St6 in Fig. 4a, red line).

## Harmonic Analysis Results

The harmonic analyses of water elevation at each station indicate that the signal is largely dominated by the semi-diurnal period band (Fig. 6). The semi-diurnal tidal species represent $\sim$ 85% of the signal at the mouth (and inner shelf), as previously reported based on longer time series (Garel and Ferreira 2013), decreasing moderately upstream until St6 (72%). A more pronounced drop ($\sim$ 10%) is noted between St6 and St7 in relation to the strong deformation of the tide induced by the sill near the estuary head (Fig. 5). The reduction of the semi-diurnal band contribution to the water level along the estuary was counter-balanced by a growth of the short period band due to the transfer of tidal energy to the quarter- and sixth-diurnal overtides. The influence of the other constituents (diurnal and higher frequencies) on the water level was small (< 10%) and varied little along the estuary.

In detail, the tidal constituents at the estuary entrance correspond to the typical values observed along the western Iberian coastline (see Quaresma and Pichon 2013). The Q1
main diurnal components ($Q_1$, $O_1$, and $K_1$) were weak (< 0.08 m) and relatively constant along the channel, with a phase that grew nearly linearly towards the estuary head (Fig. 7a, d). Amplitude variations along the estuary of the main semi-diurnal components ($M_2$, $N_2$, and $S_2$) are similar



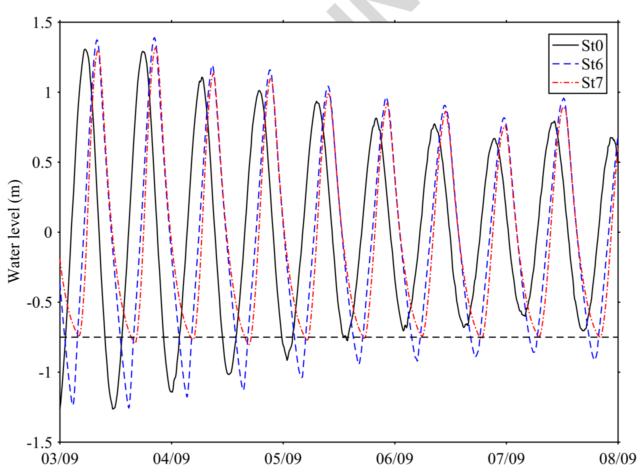


**Fig. 5** Tidal water level variations during one week at St0 (black), St6 (blue), and St7 (red). The horizontal dashed line indicates the truncation level produced by a sill between St6 and St7

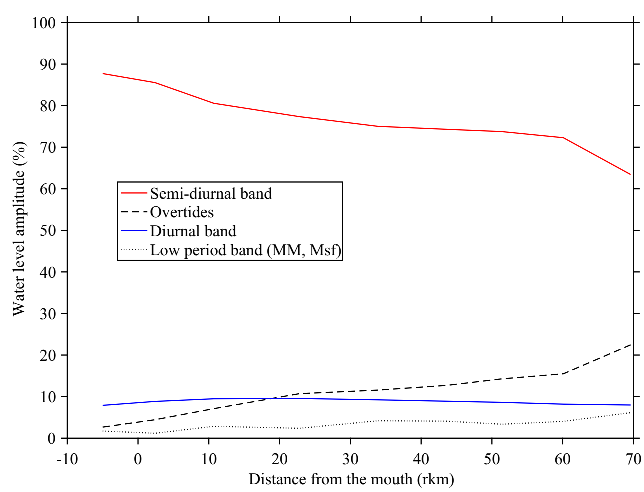


**Fig. 6** Contribution (%) of the low (mainly MM and Msf, dotted line), diurnal (blue line), semi-diurnal (red line), and high (mainly $M_4$ and $M_6$ overtides, dashed line) period bands to the total water level amplitude along the Guadiana Estuary

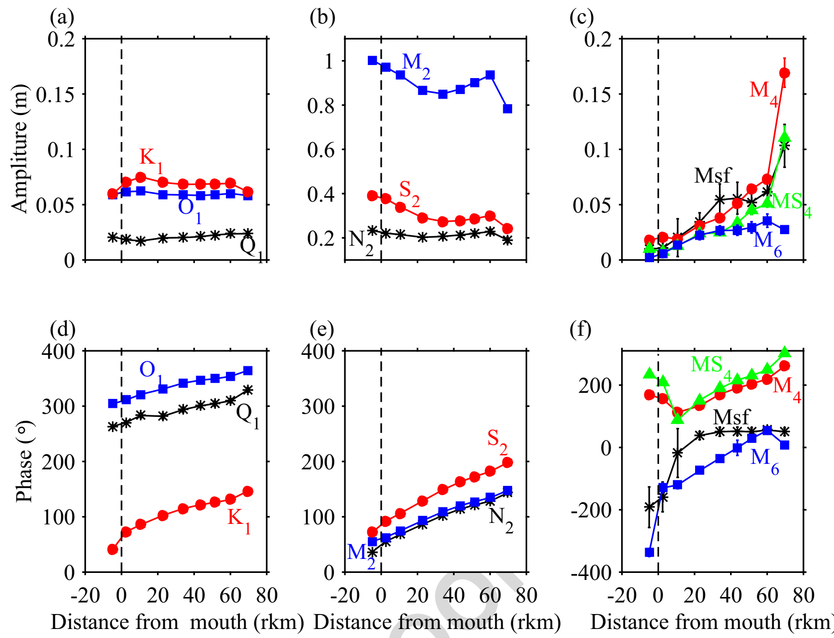


**Fig. 7** Amplitude (a, b, c, in m) and phase (d, e, f, in °, related to Greenwich) of the main constituents of the diurnal ($Q_1$, $O_1$, $K_1$), semi-diurnal ($N_2$, $M_2$, $S_2$), short ($M_4$, $MS_4$, $M_6$), and long (Msf) tidal period bands. The dashed vertical line indicates the estuary mouth (0 rkm)

to that described previously for the mean tide: damping in the lower and middle estuary, shoaling upstream until St6, where the range is close to the one at the mouth, and strong damping (due to sill-induced truncation) near the head (Fig. 7b). The $M_2$ constituent had the strongest amplitude throughout the entire estuary. The relatively large $S_2$ constituent is responsible for the pronounced spring-neap variations in tidal wave height in the region. The phase variations of $M_2$, $N_2$, and $S_2$ were similar to those of the diurnal components (Fig. 7e). The main overtides ($M_4$, $MS_4$, $M_6$) and compound tide (Msf) had overall weak amplitudes ($< 0.08$ m, until St6) progressively increasing along the estuary (Fig. 7c). The interaction of $M_2$ with the large $S_2$ wave produces substantial $MS_4$ amplitudes. Tidal wave deformation induced by the sill near the head results in a significant growth of the quarter-diurnal and fortnightly tidal amplitudes, but did not affect $M_6$. It is also noted that the phase of the overtides increased relatively steadily when propagating upstream, whereas the phase of Msf remained constant landward of $\sim$ 20 rkm (Fig. 7f). Except for the sill-affected upper station St7, these tidal harmonics characteristics were similar to those observed along the Guadalquivir, a nearby estuary (located $\sim$ 100 km to the East) that is affected by tidal reflection at its head (Diez-Minguito et al. 2012).

## CWT Results

The CWT scaleograms confirm the temporally averaged results obtained with the harmonic analyses and provide information about their temporal variability (Fig. 8). Generally, the semi-diurnal species $D_2$ largely dominates and decreases slightly towards the head; $D_1$ is relatively constant and both the quarter-diurnal ($D_4$) and sixth-diurnal ($D_6$) species grow landward. Upstream of the sill (St7), the amplitude of $D_4$ is strongly amplified and $D_6$ waves are virtually dampened out. The fortnightly tide is marked by a broad horizontal band at periods between 8 and 16 days (i.e., 0.125 to 0.0625 cycles per day) which amplitude grows upstream.

Temporal variability with the tidal forcing is observed in the short (daily and lower) period bands, characterized by weaker (stronger) amplitude at neap (spring) tide. The differences between spring and neap in $D_2$ tides tend to reduce upstream, but increase for the $D_4$ and $D_6$ overtides. Monthly variations between consecutive spring tides are also evidenced, particularly for the $D_2$ and $D_4$ species (see for example the largest spring tide around day 30 in Fig. 8). In the $D_4$ band, the time-varying contribution of the $M_4$ and $MS_4$ overtides implies large differences in the relative distortion of the tidal wave between spring (strongly deformed) and neap (weakly deformed). The friction induced by the sill near the head is strongest at spring than at neap and reduces significantly the time variability of the $D_2$ wave.

## Analytical Model

### $M_2$ Tide

The analytical solutions for both infinite and semi-closed channels were used to explore the main physical properties

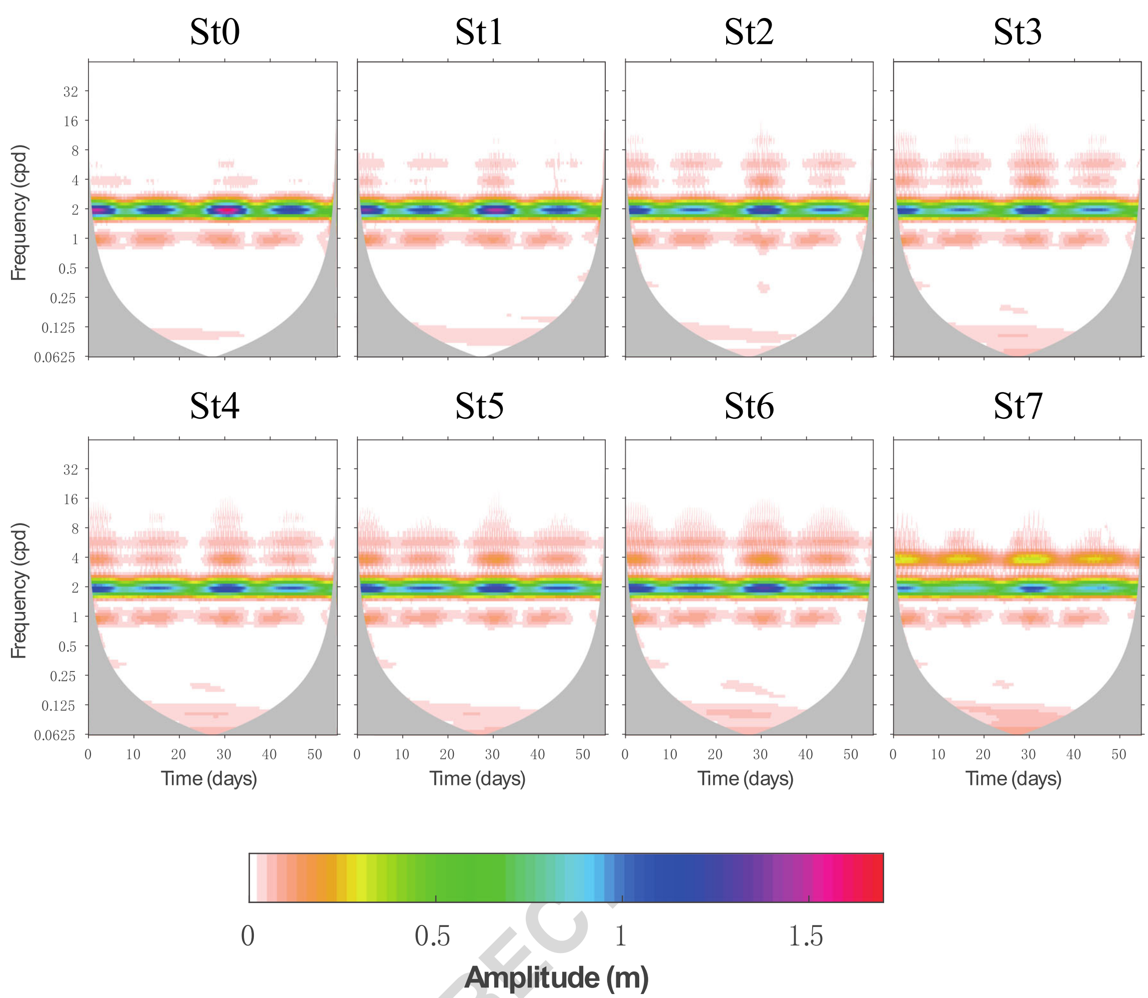


**Fig. 8** Continuous wavelet transform scaleograms of the water level amplitude (m) for St0 to St7. The white dashed line on each graph indicates the limit of the cone of influence, where edge effects become important



of a tidal wave propagating along the Guadiana Estuary. The estuarine geometry is represented with a constant mean depth (5.5 m) and a width convergence length of $b = 38$ km. The focus was on the dominant $M_2$ component (hence excluding nonlinear interactions between constituents), which has a similar amplitude to the mean tide along the channel (compare Fig. 4a with Fig. 7b). Calibration of the model against observations yielded a Manning-Strickler coefficient $K$ of 40 $m^{1/3}$ $s^{-1}$. The results are presented in Fig. 9, together with available $M_2$ observations derived from harmonic analyses.

The correspondence of the semi-closed channel model predictions with observed tidal elevations is good (Fig. 9a, solid black line). In particular, the shoaling observed upstream of 30 rkm was reproduced, whereas the model without reflection predicted continuous damping of the tidal wave along the channel (Fig. 9a, dashed black line). The phase of the $M_2$ elevation was relatively similar in both cases (except near the head) and corresponded relatively well to the observations (Fig. 9a, red lines).

The velocity amplitudes predicted by the infinite and closed-end channel solutions displayed marked differences upstream of 40 rkm (Fig. 9b, black), characterized by a (weak) significant damping towards the head when (no) reflection was considered. Section-averaged velocity measurements were not available for comparison with these model results. The infinite channel solution exhibited steady growth of the velocity phase along the estuary; in contrast, the closed-end channel solution predicted an asymptotic growth towards a limit of 45° at the head, which matches well the observations (Fig. 9b, red lines).

Finally, the results with reflection also correspond remarkably well to the observed increase in the phase lead along the estuary (depicting a standing wave behavior near the head), contrary to the (almost constant) value obtained in the case without reflection (Fig. 9c). The difference in phase lead between these two solutions increased significantly along the channel, being $\sim 10°$ at 30 rkm and $\sim 35°$ near 60 rkm.

The good correspondence between the observations and outputs from the semi-closed channel solutions indicates

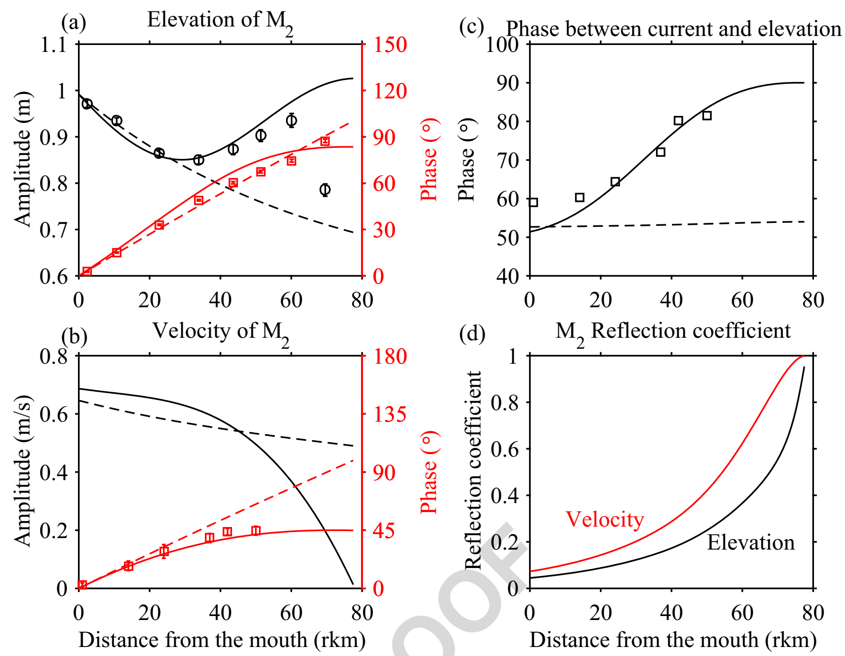


**Fig. 9** Analytical model results for an infinite channel (dashed lines) and a closed end channel (solid lines), and comparisons with observations (markers): a, amplitude (black, m) and phase (red, °) of the $M_2$ water elevation; b, velocity amplitude (black, m/s) and phase (red, °); c, phase lead (°) between the current and elevation; and, d, $M_2$ reflection coefficients for the water elevation (black) and velocity (red)

the occurrence of tidal wave reflection at the Guadiana Estuary. The results of the models with and without reflection are similar at the lower reach of the estuary, but display increasing differences towards the head. Such a pattern indicates an increasing influence of reflection on the wave properties towards the upper reach. In agreement, the reflection coefficients of the elevation and velocity amplitudes are both increasing exponentially along the estuary, being relatively weak from the mouth up to $\sim$ 40 rkm and reaching a maximum value at the closed end (as expected, see Fig. 9d). Furthermore, the reflection is stronger for the tidal velocity than the elevation. For example, at 60 rkm the wave reflection accounts for 60% of the $M_2$ velocity amplitude and 36% of the $M_2$ elevation amplitude.

## Spring-Neap variability

Differences in tidal propagation and reflection between spring and neap are evaluated with the analytical solutions for a semi-closed channel. An $M_2$ tidal period (12.42 h) was considered, along with the low neap and high spring tides described in section 4.1.1 (Fig. 4a). The analytical model reproduces correctly the observed $D_2$ wave heights at both spring and neap tides with a Manning-Strickler coefficient $K = 47$ m$^{1/3}$s$^{-1}$ (Fig. 10a). This calibration value is distinct from the one obtained for the astronomical $M_2$ tide (40 m$^{1/3}$s$^{-1}$) because $D_2$ is formed by several constituents which nonlinear interactions affect the effective friction experienced by the wave (Prandle 1997).

The velocity amplitude of the $D_2$ tide predicted by the calibrated model decayed exponentially towards a null value at the head and was much larger at spring tide than neap tide (Fig. 10b). The neap tide velocity remained relatively constant (approximately 0.6 m/s) from the mouth to $\sim$ 40 rkm, whereas the spring velocity was at a maximum at the mouth (> 1 m/s). These magnitudes are consistent with section-average measurements obtained at the lower estuary: approximately 0.9 m/s for a (spring) tidal amplitude of 1.5 m (i.e., weaker than considered here) and 0.6 m/s for a (neap) tidal amplitude of 0.6 m (see Garel and Ferreira 2013; Teodosio and Garel 2015). The phase between current and elevation was stronger at neap tide, with neap-spring differences up to 10° (equivalent to 20 min) along the downstream half of the estuary, reducing to zero towards the head (Fig. 10c).

The damping coefficients, defined in Table 1, provide insights about the fortnightly differences in semi-diurnal tidal patterns (Fig. 10e, f). The water elevation of $D_2$ at neap was continuously amplified ($\delta_A > 0$), with minimum values at the boundaries and maximum values in the mid-estuary. By contrast, the wave height in spring was significantly damped along the downstream half of the estuary (in particular near the mouth) and was slightly amplified along its upstream half. Note that along the latter section, the damping/amplification number for the water level $\delta_A$ was similar at both neap and spring tides. Likewise, the amplitude of the velocity was opposite at neap (amplification as $\delta_V > 0$) and spring tides (damping as $\delta_V < 0$) at the lowest reach of the estuary, but exhibited similar strong damping upstream (as the velocity tended towards zero at the head). Overall, the $D_2$ wave is less damped at neap than at spring and thus better reflected at the head, as indicated by the reflection coefficients in

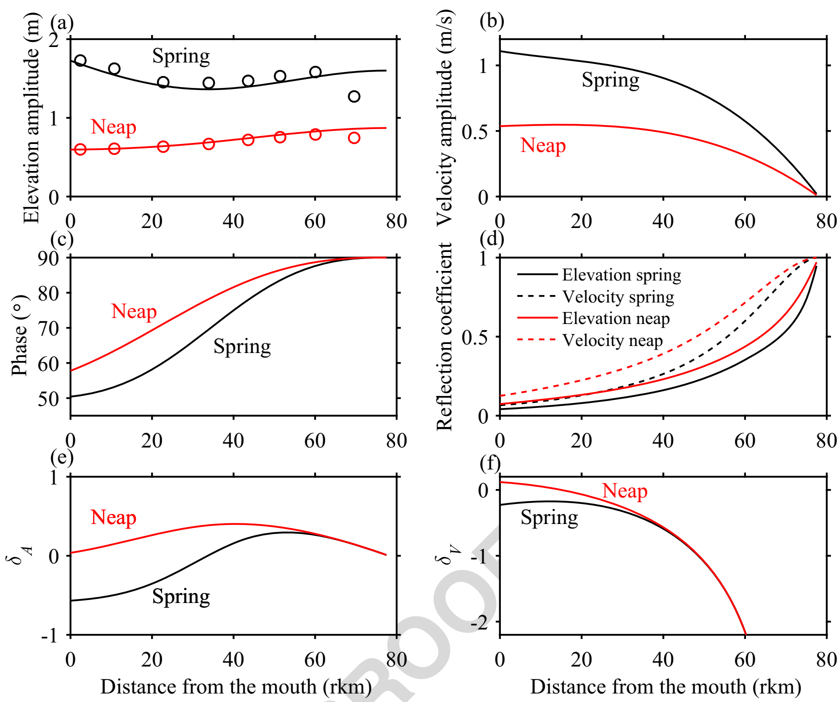


**Fig. 10** Results of the analytical solutions considering a semi-closed channel forced by neap (red lines) and spring (black lines) $D_2$ tides at the mouth: a, elevation amplitude (m) along with observations (circles); b, velocity amplitude (m/s); c, phase lead (°) between the current and elevation; d, reflection coefficients for the water elevation (solid lines) and velocity (dashed lines); e, damping number for the water level; and f, damping number for the velocity

Fig. 10d. However, spring-neap forcing variations mainly affect the tidal properties along the first (downstream) half of the estuary.

## Discussion

### Friction Versus Convergence

The good match between observations from St0 to St6 and the outputs from the semi-closed model of a convergent system with constant depth indicates that this setting is adequate to describe the main tidal properties along most of the Guadiana Estuary length. The discrepancies at St7 (Figs. 9 and 10) may be attributed to bed shoaling and partial reflection due to the bed slope and cross-channel obstructions near the head (see Fig. 2). These morphological details were not implemented in the model, and tidal dynamics along the upper ∼ 15 km of the estuary will not be addressed in the following discussion. Nevertheless, it should be noted that increased friction experienced by a wave propagating in shallowing water produces a large damping while partial reflection increases the wave amplitude near the reflection point (e.g., Familkhalili and Talke 2016; Jay 1991). The strong damping observed at St7 suggests that frictional effects induced by bed shoaling dominate the effect of partial reflection in this area.

The tidal wave amplitude and characteristics resulting from the analytical framework used in this study depend on the relative importance of convergence (represented by the shape number $\gamma$) and friction (represented by $\chi$). Since the storage ratio and mean water depth were both set to a constant value at the Guadiana Estuary, the shape number was also constant ($\gamma$ = 1.4) along the channel. The main difference between the various solutions obtained previously relates to the friction term. Comparisons of the model results with observations indicate that reflection at the estuary head has significant effects on tidal dynamics upstream of ∼ 40 rkm (Fig. 9). In this sector, reflection reduces the friction that is experienced by the propagating wave compared with the infinite channel case, resulting in wave shoaling as morphological convergence predominates over friction. Reflection influence is limited to the upper estuary due to the rapid damping of the reflected wave by friction and channel divergence as it travels downstream (Diez-Minguito et al. 2012, e.g., Park et al. 2017). In the downstream half of the estuary, the tidal dynamics can be described as a single forward propagating wave which properties are typically controlled by the balance between convergence and friction (Savenije et al. 2008). Along this estuary stretch, the mean wave was slightly damped, indicating the predominance of friction. Previous studies have reported a significant increase in wave height induced by reflection along upper estuaries limited landward by a weir such as the Ems (Schuttelaars et al. 2013) or by a dam such as the Guadalquivir (Diez-Minguito et al. 2012). Although non-linear tidal wave interactions are out of the scope of the present study, it is worth noting that reflection is associated to an increase of the amplitude of the $M_4$ overtide at these settings affecting tidal velocity asymmetries with large consequences in terms of sediment dynamics along the entire estuary (Chernetsky et al. 2010; Diez-Minguito et al. 2012).

To better understand the influence of channel convergence (represented by the estuary shape number $\gamma$), a sensitivity analysis on the mean water depth was carried out, where larger depth $\overline{h}$ corresponds with larger $\gamma$ (mimicking the effect of deepening, e.g., dredging of navigational channel). The analytically computed four dimensionless parameters ($\delta_A$, $\lambda_A$, $\mu$, and $\phi$) are illustrated along the estuary axis for a water depth of 4, 5.5, and 7 m, corresponding to an estuary shape number $\gamma$ of 1.2, 1.4, and 1.6, respectively (Fig. 11). The longitudinal tidal amplitude, velocity amplitude, and phase difference between velocity and elevation are increased with the estuary shape number $\gamma$ (hence larger $\delta_A$, $\mu$, and $\phi$, see Fig. 11a, c, d). As expected, the celerity number $\lambda_A$ is decreased as $\gamma$ increases (Fig. 11b), indicating a larger wave speed. Upstream of 40–60 rkm, $\delta_A$ decreases for all $\gamma$ cases as it converges towards zero at the head, depicting an inverse behavior than downstream (i.e., larger $\delta_A$ for smaller $\gamma$). This is due to the additional impact from the reflected wave, apart from the channel convergence and bottom friction. Accordingly, $\delta_A$ starts to decrease further from the head for larger shape number, when the wave is less damped and thus better reflected than with smaller shape numbers. It is also noted that the variability patterns of $\delta_A$ with the shape number (or depth) and with the tidal forcing amplitude are similar (Figs. 10e and 11a). In particular, $\delta_A$ is equal at neap and spring along the upper half of the estuary, but is stronger and starts to decreases further form the head at neap due to reduced friction. The main differences in wave properties are observed between the mouth and 30 rkm, where shoaling at neap tide (convergence dominates) and damping at spring tide (friction dominates) relate to the nonlinear increase in bottom resistance with tidal flow velocity (Fig. 10).

Overall, the tidal amplitude was more or less constant along the entire channel, with variations of less than 10% on average, whereas it would be damped in the absence of reflection. Estuaries with approximately constant tidal amplitude are often referred to as "ideal" estuaries (Pillsbury 1940). Most of these systems consist of coastal plain estuaries with constant depths and smooth transitions with the river that hamper tidal wave reflection at the head (Savenije 2012). At convergent ideal estuaries, both the wave celerity and phase lead (between 0 and 90°) are constant because the energy that is gained from morphological convergence is balanced with the energy lost by friction as the wave travels upstream (Jay 1991; Friedrichs and Aubrey 1994; Savenije and Veling 2005; van Rijn 2011). In the Guadiana Estuary, the tidal amplitude is relatively constant along the channel, but the phase lead varies significantly (from 50° at the mouth to 90° near the head) in the presence of reflection (Fig. 9a, c). In the same way, the semi-diurnal wave celerity (from the $M_2$ phase) displays strong variations, ranging from $\sim$ 5 m/s near the mouth to almost double at 60 rkm (Fig. 12, blue line). Both analytical solutions (infinite and semi-closed channels) reasonably represent the wave celerity observed in the lower and middle estuary where the effect of reflection is weak (Fig. 12). By contrast, the wave acceleration in the upper estuary is only predicted by the semi-closed model. Hence, despite constant tidal amplitude along its length, the Guadiana Estuary does not fit the

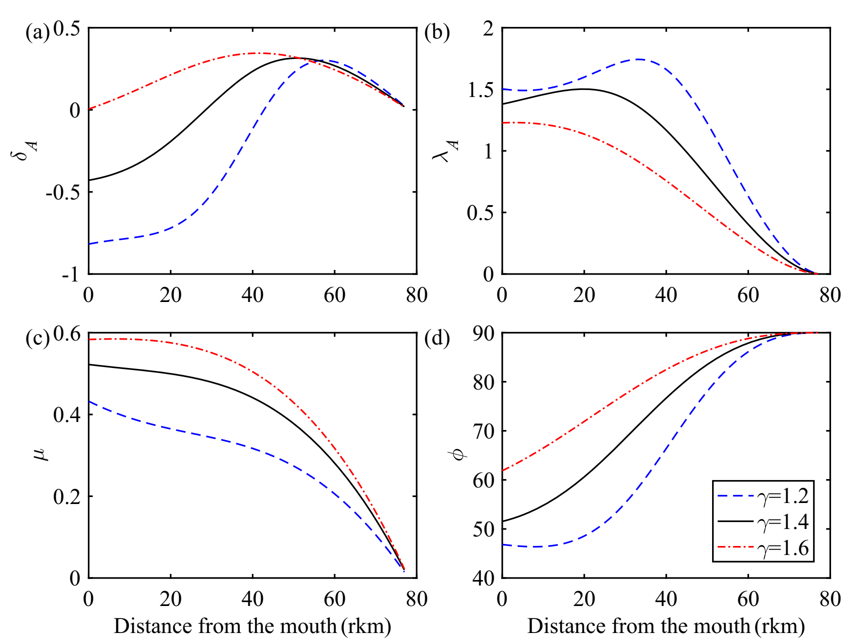


**Fig. 11** Longitudinal variations of the analytically computed damping/amplification number $\delta_A$ (**a**), celerity number $\lambda_A$ (**b**), velocity number $\mu$ (**c**), and phase lead $\phi$ (**d**) for given different estuary shape number $\gamma$

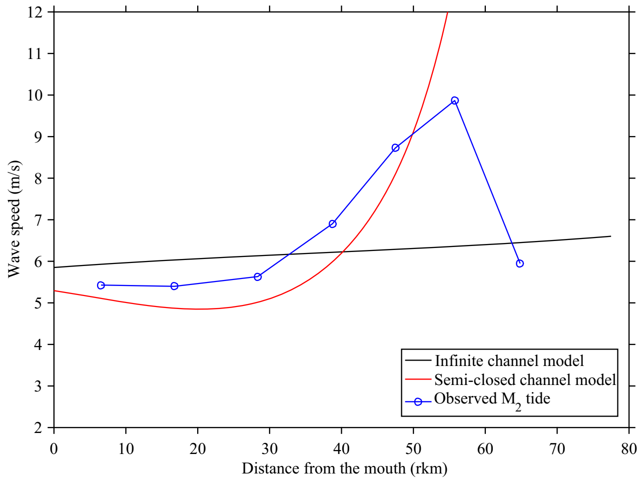


**Fig. 12** Semi-diurnal wave celerity (m/s) along the estuary (km) from observations (blue) and model results considering a $M_2$ tide propagating along an infinite channel (black line) and semi-closed (red line) channels

definition of an ideal estuary in terms of wave celerity and phase lead because of reflection effects. Assuming an ideal case may draw large inaccuracies. In particular, the difference in phase between velocity and elevation is one of the most important parameters in describing tidal wave propagation along estuaries (Savenije and Veling 2005).

## Tidal Amplitude Forcing and Wave Speed

The previous "Friction Versus Convergence" reported large changes in the $M_2$ wave celerity along the estuary. In the present section, the influence of tidal amplitude variations at the mouth is examined considering the wave celerity derived from the travel time of both high (HWL) and low (LWL) water levels during the spring and neap tides analyzed previously. These observations are compared with the celerity ($c$) predicted by the semi-closed model for a $D_2$ wave. A strong mean slope of the water level, for example of $O(10^{-5})$ along the Columbia River estuary, can affect the upstream propagation of the tide (see Jay and Flinchem 1997; Jay et al. 2011, 2015). Along the Guadiana Estuary, the slope results mainly from the Stokes transport and is of $O(10^{-6})$, i.e., one order of magnitude lower than the slope of the propagating tidal wave (see below and Garel and Ferreira 2013). Thus, the effect of the mean slope on the tidal circulation is neglected. To account for differences induced by the tidal stage, the celerity at low ($c_{\text{LWL}}$) and high ($c_{\text{HWL}}$) water level were obtained as follows (Savenije 2012):

$$c_{\text{HWL}} = c\sqrt{\frac{1+\eta}{h}} + \upsilon \sin(\pi/2 - \phi)\,, \qquad (21)$$

and

$$c_{\text{LWL}} = c\sqrt{\frac{1-\eta}{h}} - \upsilon \sin(\pi/2 - \phi)\,. \qquad (22)$$

For a small tidal amplitude to depth ratio, it can be seen from Eqs. 21 and 22 that the direct effect of the water level fluctuation on the wave celerity will be small, but for large amplitude waves, the wave celerity between HWL and LWL can differ substantially.

The observations and model outputs indicate similar trends (Fig. 13), with relatively constant celerity in the lower and middle estuary, and acceleration upstream due to the increasing standing wave behavior of the $D_2$ tide towards the head. This acceleration occurs at a shorter distance from the mouth at neap than at spring tide because this wave is better reflected and has as such a phase lead closer to 90° (Fig. 10c). In detail, the agreement between the model and observations is very good at spring tide, with both $c_{\text{HWL}}$ and $c_{\text{LWL}} < c_0$ downstream of $\sim$ 50 rkm. At neap tide, the measured wave celerity was approximately equals to $c_0$ (in particular for $c_{\text{LWL}}$), in agreement with the model results in the lower and middle estuary, whereas the discrepancy increased upstream. The upstream discrepancies are attributed to frictional effects along the upper $\sim$ 15 km of the channel, not considered in the model (these discrepancies are larger at neap tide, when the predicted reflection is stronger). Overall, both the observations and the model agreed that the $D_2$ wave travels faster at neap than at spring tide from the mouth to $\sim$ 60 rkm, at least.



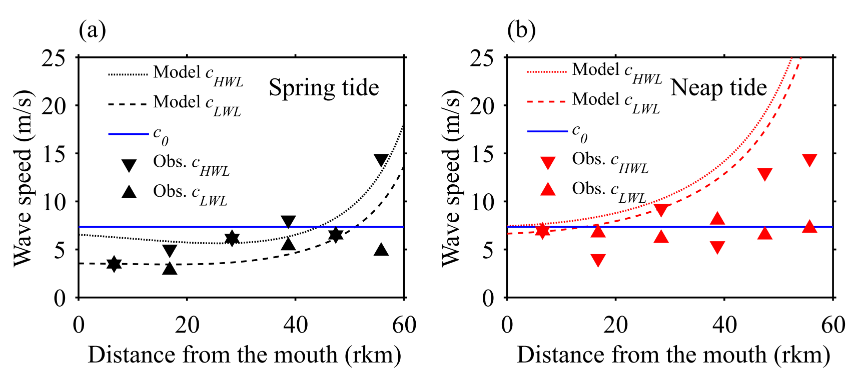


**Fig. 13** Wave celerity (m/s) along the estuary (rkm) at (**a**) spring and (**b**) neap tides from measurements (HWL: downward triangles; LWL: upward triangles) and from analytical solutions (HWL: dotted line; LWL: dashed line). The blue line indicates the classical wave celerity $c_0$. The star symbol results from the overlap of the up-pointing triangle with down-pointing triangle

Mean water levels in estuaries are generally largest at spring tide due to nonlinear effects. For example, the mean water level of the specific spring tidal cycle considered in this study was up to ∼ 40 cm higher than the neap one (Fig. 14). Since the velocity is related to the water depth, semi-diurnal tidal waves at spring could be considered the fastest. This is not always the case, as tidal damping also affects wave celerity (Savenije et al. 2008; Savenije and Veling 2005). With the analytical framework used in this study, the scaled celerity equation for an infinite channel takes the following form (Savenije 2012):

$$c^2 = \frac{c_0^2}{1 - \delta_A(\gamma - \delta_A)} . \qquad (23)$$

Equation 23 is used herein to clarify the relationship between wave damping and celerity. When reflection is considered, this relationship is not as explicit but results in similar trends (see Cai et al. 2016; Park et al. 2017). The term $\delta_A(\gamma - \delta_A)$ is the damping term. Its maximum value is 1, corresponding to a situation of "critical convergence" which is the transition to an apparent standing wave, i.e., an incident wave with infinite wave celerity mimicking a standing wave pattern (Jay 1991). As illustrated in Fig. 15, the wave celerity equals the classical wave celerity $c_0$ in two cases: (1) in ideal estuaries, where there is no damping or amplification ($\delta_A$ =0) because convergence is exactly balanced by friction; (2) in estuaries where the shape number equals the damping number ($\gamma = \delta_A$). In the latter case, a wave is always amplified (since $\gamma$ is always positive) but convergence and acceleration are equal and cancel each other out. When the wave is damped ($\delta_A < 0$), the wave celerity from Eq. 23 is less than $c_0$ (Fig. 15). When the wave is amplified ($\delta_A > 0$), the wave celerity is generally greater than $c_0$, except for the singular situation where $\delta_A > \gamma$. The latter case generally corresponds to systems of hundreds of kilometers in length that are many tens of meters deep, such as the Gulf of Maine and the Bristol Channel (Friedrichs and Aubrey 1994; Prandle and Rahman 1980).

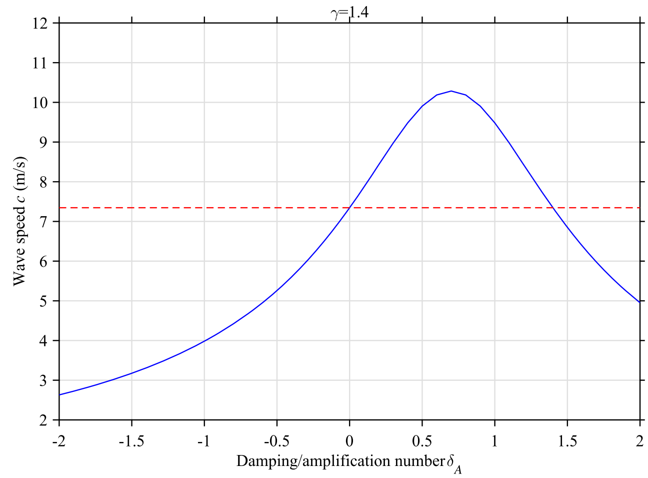


**Fig. 15** Relationship between the damping/amplification number ($\delta_A$) and wave speed in an infinite channel with shape number ($\gamma$) equal to 1.4. The dashed red line represents the classical wave celerity $c_0$

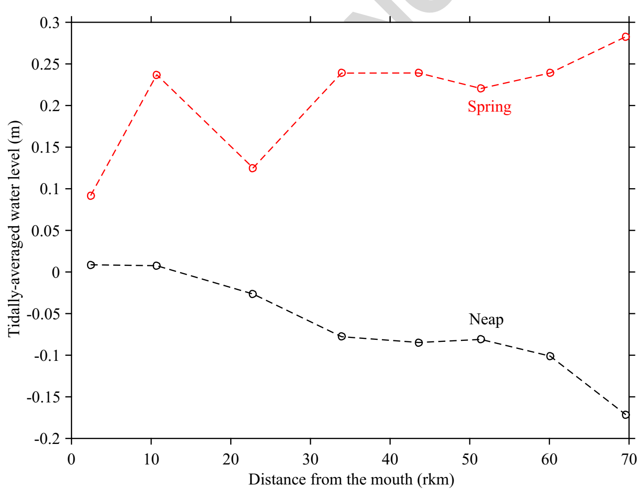


**Fig. 14** Mean water level (m) at stations along the estuary at spring tide (31 August 2015, red) and neap tide (23 August 2015, black) and low (< 50 $m^3s^{-1}$) freshwater inflows. The dashed line is an interpolation between measurements (circles)

As with the infinite channel case, wave damping in the presence of reflection explains the variations in wave celerity that were observed along the Guadiana channel as a function of $D_2$ amplitude at the mouth. The wave damping number ($\delta_A$) and celerity number ($c_0/c$) obtained by the closed-end solutions are represented in Fig. 16. Near the mouth, the wave is damped and its celerity is smaller than $c_0$, in particular for large tidal amplitudes. Amplification of the wave propagating upstream leads to a situation where $c$ is greater than $c_0$. From the mouth to ∼ 60 rkm, the damping factor $\delta_A$ is notably larger at neap than at spring tide, resulting in a comparatively faster tidal wave (Fig. 16).

## Resonance Behavior

Previous results have shown that reflection at the upstream boundary affects the dynamics of the daily tide at the Guadiana Estuary. Following Cai et al. (2016), the analytical solutions for a semi-closed channel were implemented to explore the relationship between the tidal period (between 1 and 40 h) and the resonance behavior along the channel. The forcing amplitude at the sea boundary was set to a constant value, equal to the amplitude of the $M_2$ tidal component (0.98 m). Tidal amplitude variations at the mouth (0.6 m in neap and 1.5 m in spring tide) were also examined since their effects upon wave celerity (reported in "Tidal Amplitude Forcing and Wave Speed") are likely to affect the resonance characteristics. It is also noted that the interaction of the $M_2$ constituent with other constituents of the $D_2$ wave

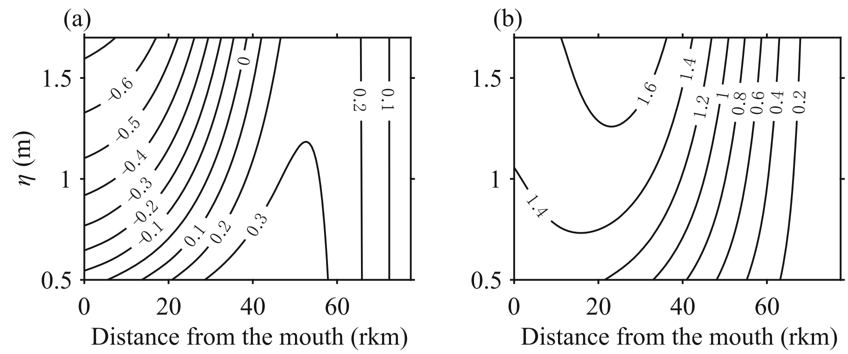


**Fig. 16** Variation in (**a**) the damping/amplification number $\delta_A$ and (**b**) celerity number $\lambda$ ($=c_0/c$) with $D_2$ tidal amplitude $\eta$ (m) along the Guadiana Estuary

(in particularly $S_2$) induces some small variations in the semi-diurnal tidal wave period between neap and spring that could induce distinct resonance behaviors (Dronkers 1964).

It is important to note that pure tidal resonance only occurs in a frictionless case. Considering only water levels, antinodes are those points where the tidal amplitude is maximum. For the frictional case, the antinodes are identified by the condition of $\delta_A$=0, corresponding to maximum amplitude. Hence, in this paper, tidal resonance is considered to occur for a period that corresponds to the largest tidal amplitude at the head with $\delta_A$=0. The resonance defined in this way is biased towards long periods, which are less damped than shorter ones (and have therefore stronger influence on the wave amplitude at the head). The obtained resonance period should therefore be considered as an upper limit. In addition, the analytical model does not include the sill and small weir near the head, which probably affect the resonance process. However, as discussed previously, the model is able to represent the tidal properties along most of the estuary length (from the mouth to St6), allowing to examine resonance effects along this stretch (e.g., 0–60 rkm), at least in a qualitative way. The incident and reflected waves have distinct phases such that the sum of their amplitudes is not necessarily equal to the total amplitude (hence, their maximum height at the head may be distinct from the resonance period). To compare their response to distinct tidal amplitude forcing, the height of both the incident and reflected waves is normalized to their (incident and reflected) amplitudes at the mouth and at the head, respectively.

For an $M_2$ tide amplitude, the Guadiana Estuary resonates at a (maximum) period of 20 h (Fig. 17a). The phase between current and elevation increases with the tidal period, resulting in a standing wave system for a periodicity > 30 h with a nearly 90° phase lead along the entire estuary (Fig. 17b). The phase also increases from the mouth to the



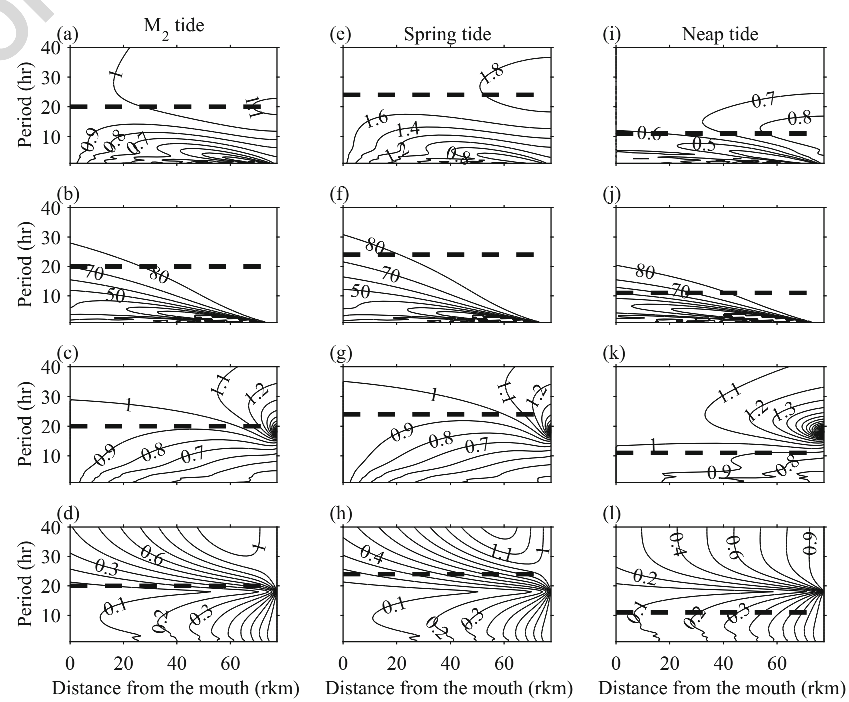


**Fig. 17** The main tidal wave parameters along the Guadiana Estuary (*x*-axis, km) as a function of the tidal periods (*y*-axis, h) under various forcing amplitudes at the mouth: $M_2$ tide (left), spring tide (middle), and neap tide (right): amplitude (m) of tidal elevations (**a**, **e** , **i**); phase lead (°) between current and elevation (**b**, **f**, **j**); normalized amplitude (m) of the incident wave (**c**, **g**, **k**); and, normalized amplitude (m) of the reflected wave (**d**, **h**, **l**). The horizontal dashed line refers to the maximum resonance period, estimated from the maximum total wave amplitude at the head

head for periods > 8.5 h. From the mouth to 60 rkm, the incident wave shoals along the channel for periods larger at 25 h but is damped—in particular downstream of 30 rkm—for shorter periods (Fig. 17c). These distinct patterns (e.g., shoaling and damping of the diurnal and semi-diurnal tidal wave, respectively) illustrate the frequency-dependent response of estuaries to tidal forcing (Prandle and Rahman 1980). This phenomenon is explicitly formulated in the analytical model, where both convergence and frictional dissipation are related linearly to the tidal period (Table 1; Cai et al. 2016). As previously observed for an $M_2$ tidal period (Fig. 9d), the amplitude of the reflected wave decreases rapidly from the head as it travels downstream due to friction and channel divergence (Fig. 17d). For any of the periods examined, the contribution of the reflected wave to the total tidal amplitude is restricted to the upper reach of the estuary, being, for instance < 0.1 m in absolute amplitude downstream of 30 rkm (not shown).

For spring tide amplitudes, the wave patterns are similar to those in the $M_2$ case, indicating that the main tidal properties are not strongly modified when the tidal amplitude at the mouth varies between its mean and maximum values (Fig. 17a, h). Hence, the wave patterns results along the estuary are expected to vary little in function of monthly spring tide amplitude variations caused by contributions of the $O_1$ and $K_1$ constituents. Amplitude variations at the mouth at neap (e.g., 0.6 m at minimum and 0.7 m in average) are not as strong as at spring and the results of Fig. 17i, l are considered representative of weak (neap) amplitude forcing in general. At spring, the maximum wave height at the head is obtained for a maximum period of 24 h (Fig. 17e). For neap tide amplitudes, resonance occurs for a maximum period of 11 h, hence shorter than the semi-diurnal periodicity (Fig. 17i). These differences in resonance period with tidal elevation forcing are related to the distinct friction—hence celerity—discussed in “Tidal Amplitude Forcing and Wave Speed.” It was verified that there is no significant difference in the results due to small changes of the period within a tidal band. In particular, variations in the daily wave period between spring and neap have considerably lesser effects on the wave properties than the wave height forcing (e.g., compare Fig. 17g, k for periods between 10 and 15 h). This justifies using similar ($M_2$) frequency for both spring and neap forcing. Providing that the estuary is relatively close to resonance, reduced effects of small wave period variations suggest strong friction within the reflectance zone (Dronkers 1964).

The phase lead variations of the neap and spring $D_2$ tides are similar to those of the $M_2$ tide, except that a standing wave develops for relatively shorter and longer tidal periods for the neap and spring wave height, respectively (Fig. 17f, j). The normalized amplitudes of the incident wave vary with friction, with enhanced damping and reduced shoaling for spring forcing (strong friction) compared to neap forcing (weak friction; Fig. 17g, k). Around the semi-diurnal period the incident wave is relatively constant along the entire estuary at neap and upstream of ∼ 40 rkm at spring tide (see the flatten isocontours in Fig. 17g, h), indicating a balance between the frictional effects and geometric convergence (Dyer 1997; Savenije and Veling 2005), which contribute (together with reflection) to the reported wave shoaling at the upper reach. The reflected wave is rapidly damped along the channel, except for periods > 30 h (Fig. 17h, l). Below the diurnal period, the normalized reflected wave height is highly similar for all of the forcing amplitudes considered, being marginally larger in the neap tide (Fig. 17d, h, i). However, under spring forcing the absolute reflected wave height is larger at the head and thus along the channel (not shown).

## Conclusions

Tidal wave propagation in the 78-km-long narrow convergent Guadiana Estuary was examined based on observations and analytical solutions. An analytical model was implemented, where the complex geometry (weirs and sill) landward of ∼ 65 rkm was represented by a single closed boundary. The results of the model compare well to observations of elevation and phase lead from the mouth to 60 rkm and indicates reflection of the tidal wave at the head of the estuary.

The natural resonance period of the estuary is 20 h, at maximum. For shorter periods, the influence of reflection is restricted to the upper estuary, with reflection coefficients < 0.2 downstream of 50 rkm, because of the damping of the reflected wave by friction and channel divergence as it travels downstream. Along the lower half of the estuary, the tidal dynamics can be described as a single wave propagating upstream, characterized by tidal properties that are typically controlled by the balance between morphological convergence and friction. The $M_2$ incident wave is damped along this stretch (friction dominates over convergence), but have an approximately constant height along the upper reach (friction and convergence are almost balanced). Reflection reduces the friction experienced by the propagating $M_2$ wave. Along the upper reach, this effect combines with enhanced morphological convergence and results in the overall amplification of the tidal wave (convergence dominates over friction). Damping downstream and shoaling upstream are relatively minimal (< 10% variations), such that the estuary could be considered as “ideal.” However, this concept may entail incorrect assumptions when applied to the Guadiana Estuary because of the effect of reflection on the wave celerity and phase lead.

Significant variations in the properties of the propagating $D_2$ (semi-diurnal) wave were observed between spring and neap tides. The cases with spring and $M_2$ amplitude forcing are highly similar indicating comparable dynamics of the propagating tide. Neap-spring variations are especially strong from the mouth to $\sim$ 50 rkm (damping in spring, shoaling in neap), in relation to the variable friction (weaker in neap, stronger in spring) experienced by the incident $D_2$ wave. Consequently, the semi-diurnal wave celerity is larger at neap than at spring tide (opposite to expectations based on the mean water level) and the estuary resonates at very distinct periods. These resonance periods are estimated to be shorter than the semi-diurnal periodicity at neap tide but close to the diurnal periodicity at spring tide. Upstream of 50 rkm, the influence of reflection increases significantly, but the patterns of the reflected wave vary little with amplitude forcing for short period waves ($<$ 15 h). In particular, a $D_2$ tide forced with neap and spring amplitudes at the mouth exhibit similar shoaling along the upper reach, which is produced by the combined effect of reflection (that reduces friction) and enhanced morphological convergence.

Finally, we note that the proposed method is most accurate in estuaries where the tidal amplitude to depth ratio is small and the river discharge is small compared to the tidal discharge, e.g., the Western Scheldt estuary in the Netherlands, the Delaware estuary in the USA, the Bristol Channel in the UK. Overall, this study indicates that the analytical framework presented can accurately describe the most relevant dynamic features of a tide propagating along a narrow convergent estuary, including the effect of tidal forcing variations, considering a single effective tidal wave. The method provides direct insights into the relative importance of channel convergence and bottom friction on the tidal characteristics, using simplified geometric parameters that are generally easy to determine.



**Funding Information** The work of the first author was supported by FCT research contract IF/00661/2014/CP1234, while the work of the second author was funded by the National Natural Science Foundation of China (Grant No. 51709287), the Basic Research Program of Sun Yat-Sen University (Grant No. 17lgzd12), and the Water Resource Science and Technology Innovation Program of Guangdong Province (Grant No. 2016-20).

## References

Buschman, F.A., A.J.F. Hoitink, M. van der Vegt, and P. Hoekstra. 2009. Subtidal water level variation controlled by river flow and tides. *Water Resources Research* 45. https://doi.org/10.1029/2009WR008167.

Cai, H., H.H.G. Savenije, and M. Toffolon. 2012. A new analytical framework for assessing the effect of sea-level rise and dredging on tidal damping in estuaries. *Journal of Geophysical Research* 117. https://doi.org/10.1029/2012JC008000.

Cai, H., M. Toffolon, and H.H.G. Savenije. 2016. An analytical approach to determining resonance in semi-closed convergent tidal channels. *Coastal Engineering Journal* 58. Artn 1650009 https://doi.org/10.1142/S0578563416500091.

Chernetsky, A.S., H.M. Schuttelaars, and S.A. Talke. 2010. The effect of tidal asymmetry and temporal settling lag on sediment trapping in tidal estuaries. ~~*Ocean Dynam.*~~ 60: 1219–1241. https://doi.org/10.1007/s10236-010-0329-8.

Codiga, D.L. 2011. *Unified tidal analysis and prediction using the Utide Matlab functions. Graduate School of Oceanography University of Rhode Island*. Narragansett G: RI.

Diez-Minguito, M., A. Baquerizo, M. Ortega-Sanchez, G. Navarro, and M.A. Losada. 2012. Tide transformation in the Guadalquivir estuary (SW Spain) and process-based zonation. *Journal of Geophysical Research* 117. https://doi.org/10.1029/2011jc007344.

Dronkers, J.J. 1964. *Tidal computations in River and Coastal Waters*. New York: Elsevier.

Dyer, K.R. 1997. *Estuaries: a physical introduction*, 2nd edn. Chichester: U.K.

Familkhalili, R., and S. Talke. 2016. The effect of channel deepening on tides and storm surge: a case study of Wilmington, NC. *Geophysical Research Letters* 43. https://doi.org/10.1002/2016GL069494.

Flinchem, E., and D. Jay. 2000. An introduction to wavelet transform tidal analysis methods. *Estuarine, Coastal and Shelf Science* 51: 177–200. https://doi.org/10.1006/ecss.2000.0586.

Friedrichs, C.T., and O.S. Madsen. 1992. Nonlinear diffusion of the tidal signal in frictionally dominated embayments. *Journal of Geophysical Research* 97: 5637–5650.

Friedrichs, C.T., and D.G. Aubrey. 1994. Tidal propagation in strongly convergent channels. *Journal of Geophysical Research* 99: 3321–3336. https://doi.org/10.1029/93jc03219.

Garel, E., L. Pinto, A. Santos, and O. Ferreira. 2009. Tidal and river discharge forcing upon water and sediment circulation at a rock-bound estuary (Guadiana estuary, Portugal). *Estuarine, Coastal and Shelf Science* 84: 269–281.

Garel, E., and O. Ferreira. 2013. Fortnightly changes in water transport direction across the mouth of a narrow estuary. ~~*Estuar. Coast.*~~ 36: 286–299.

Garel, E., and O. Ferreira. 2015. Multi-year high-frequency physical and environmental observations at the Guadiana estuary. *Earth System Science Data* 72: 299–309. https://doi.org/10.5194/essd-7-299-2015.

Garel, E., and D. D'Alimonte. 2017. Continuous river discharge monitoring with bottom-mounted current profilers at narrow tidal estuaries. *Continental Shelf Research* 133: 1–12.

Guo, L., M. van der Wegen, D.A. Jay, P. Matte, Z.B. Wang, D.J. Roelvink, and Q. He. 2015. River-tide dynamics: exploration of non-stationary and nonlinear tidal behavior in the Yangtze River estuary. *Journal of Geophysical Research* 120: 3499–3521. https://doi.org/10.1002/2014JC010491.

Hoitink, A.J.F., and D.A. Jay. 2016. Tidal river dynamics: Implications for deltas. *Reviews of Geophysics* 54: 240–272. https://doi.org/10.1002/2015RG000507.

Hunt, J.N. 1964. Tidal oscillations in estuaries. *Geophysical Journal of the Royal Astronomical Society* 8: 440–455. https://doi.org/10.1111/j.1365-246X.1964.tb03863.x.

Jay, D.A. 1991. Green law revisited - tidal long-wave propagation in channels with strong topography. *Journal of Geophysical Research* 96: 20585–20598. https://doi.org/10.1029/91jc01633.

Jay, D.A., and E.P. Flinchem. 1997. Interaction of fluctuating river flow with a barotropic tide: a demonstration of wavelet tidal analysis methods. *Journal of Geophysical Research* 102: 5705–5720. https://doi.org/10.1029/96jc00496.

Jay, D.A., and E.P. Flinchem. 1999. A comparison of methods for analysis of tidal records containing multi-scale non-tidal background energy. *Continental Shelf Research* 19: 1695–1732. https://doi.org/10.1016/S0278-4343(99)00036-9.

Jay, D.A., K. Leffler, and S. Degens. 2011. Long-term evolution of columbia river tides. *Journal of Waterway Port C-Asce* 137: 182–191. https://doi.org/10.1061/(ASCE)WW.1943-5460.0000082.

Jay, D.A., K. Leffler, H.L. Diefenderfer, and A.B. Borde. 2015. Tidal-fluvial and estuarine processes in the lower Columbia River: i. Along-channel water level variations, Pacific Ocean to Bonneville Dam. ~~*Estuarine and Coastal*~~ 38: 415–433. https://doi.org/10.1007/s12237-014-9819-0.

Kukulka, T., and D.A. Jay. 2003. Impacts of Columbia River discharge on salmonid habitat: 1. A nonstationary fluvial tide model. *Journal of Geophysical Research* 108. https://doi.org/10.1029/2002JC001382.

Lanzoni, S., and G. Seminara. 1998. On tide propagation in convergent estuaries. *Journal of Geophysical Research* 103: 30793–30812. https://doi.org/10.1029/1998JC900015.

Lincoln, J.M., and D.M. FitzGerald. 1998. Tidal distortions and flood dominance at five small tidal inlets in southern maine. *Marine Geology* 82: 30793–30812.

Lorentz, H.A. 1926. Verslag Staatscommissie Zuiderzee (in Dutch). Technical Report. Alg. Landsdrukkerij.

Park, M.J., H.H.G. Savenije, H.Y. Cai, E. Jee, and N. Kim. 2017. Progressive change of tidal wave characteristics from the Eastern Yellow Sea to the Asan Bay, a strongly convergent bay in the west coast of Korea. ~~*Ocean Dynam.*~~ 67: 1137–1150. https://doi.org/10.1007/s10236-017-1078-8.

Pillsbury, G.B. 1940. *Tidal hydraulics. U.S. Engineer dept. Professional paper of the corps of engineers*. Washington: no. 34. U.S. Govt. Print. Off.

Prandle, D. 1997. The influence of bed friction and vertical eddy viscosity on tidal propagation. *Continental Shelf Research* 17: 1367–1374. https://doi.org/10.1016/S0278-4343(97)00013-7.

Prandle, D. 2009. *Estuaries: dynamics, mixing sedimentation and morphology*. Cambridge: Cambridge University Press.

Prandle, D., and M. Rahman. 1980. Tidal response in estuaries. *Journal of Physical Oceanography* 10: 1552–1573. https://doi.org/10.1175/1520-0485(1980)010⟨1552:TRIE⟩2.0.CO;2.

~~van~~ Rijn, L.C. 2011. Analytical and numerical analysis of tides and salinities in estuaries; part I: tidal wave propagation in convergent estuaries. ~~*Ocean Dynamic*~~ 61: 1719–1741. https://doi.org/10.1007/s10236-011-0453-0.

Sassi, M.G., and A.J.F. Hoitink. 2013. River flow controls on tides and tide-mean water level profiles in a tidal freshwater river. *Journal of Geophysical Research* 118: 4139–4151. https://doi.org/10.1002/Jgrc.20297.

Savenije, H.H.G. 1998. Analytical expression for tidal damping in alluvial estuaries. *Journal of Hydraulic Engineering* 124: 615–618. https://doi.org/10.1061/(ASCE)0733-9429(1998)124:6(615).

Savenije, H.H.G., and E.J.M. Veling. 2005. Relation between tidal damping and wave celerity in estuaries. *Journal of Geophysical Research*: 110. https://doi.org/10.1029/2004JC002278.

Savenije, H.H.G., M. Toffolon, J. Haas, and E.J.M. Veling. 2008. Analytical description of tidal dynamics in convergent estuaries. *Journal of Geophysical Research*: 113. https://doi.org/10.1029/2007JC004408.

Savenije, H.H.G. 2012. Salinity and tides in alluvial estuaries (2nd completely revised edition). Available at www.salinityandtides.com (last access: 26 December 2014).

Schuttelaars, H.M., V.N. de Jonge, and A. Chernetsky. 2013. Improving the predictive power when modelling physical effects of human interventions in estuarine systems. ~~*Ocean Coastal Manage*~~ 79: 70–82. https://doi.org/10.1016/j.ocecoaman.2012.05.009.

Shetye, S.R., and V. Vijith. 2013. Sub-tidal water-level oscillations in the Mandovi estuary, west coast of India. *Estuarine, Coastal and Shelf Science* 134: 1–10. https://doi.org/10.1016/j.ecss.2013.09.016.

Teodosio, M.A., and E. Garel. 2015. Linking hydrodynamics and fish larvae retention in estuarine nursery areas from an ecohydrological perspective. *Ecohydrology & Hydrobiology* 15: 182–191.

Toffolon, M., and H.H.G. Savenije. 2011. Revisiting linearized one-dimensional tidal propagation *Journal of Geophysical Research*: 116. https://doi.org/10.1029/2010JC006616.

Van Rijn, L. 2010. Tidal phenomena in the Scheldt Estuary - Part 1, Technical Report, The Netherlands.

Wang, Z., C. Jeuken, and H. Vriend. 1999. Tidal asymmetry and residual sediment transport in estuaries: a literature study and application to the Western Scheldt. In *Hydraulic Engineering Reports*, WL, D., 67. The Netherlands.

Wang, Z.B., J.C. Winterwerp, and Q. He. 2014. Interaction between suspended sediment and tidal amplification in the Guadalquivir estuary. ~~*Ocean Dynamic*~~ 64: 1487–1498. https://doi.org/10.1007/s10236-014-0758-x.

Winterwerp, J.C., and Z.B. Wang. 2013. Man-induced regime shifts in small estuaries-I: theory. ~~*Ocean Dynamic*~~ 63: 1279–1292. https://doi.org/10.1007/s10236-013-0662-9.

Zhang, E.F., H.H.G. Savenije, S.L. Chen, and X.H. Mao. 2012. An analytical solution for tidal propagation in the yangtze estuary, china. *Hydrology and Earth System Sciences* 16: 3327–3339. https://doi.org/10.5194/hess-16-3327-2012.

# AUTHOR QUERY

**AUTHOR PLEASE ANSWER QUERY:**

Q1. Reference Quaresma and Pichon (2013) is cited in the body but its bibliographic information is missing. Kindly provide its bibliographic information; otherwise, please delete it from the text/body.